

UC Berkeley

UC Berkeley Previously Published Works

Title

Energy-Based and Strain-Based Methods for Estimation of Pore Water Pressure within Liquefied Soil Layers

Permalink

<https://escholarship.org/uc/item/4h23r8q4>

Journal

Journal of Geotechnical and Geoenvironmental Engineering, 150(10)

ISSN

1090-0241 1943-5606

Authors

Ko, Kil-Wan

Kayen, Robert E

Publication Date

2024-10-01

DOI

10.1061/JGGEFK.GTENG-11458

Peer reviewed



Energy-Based and Strain-Based Methods for Estimation of Pore Water Pressure within Liquefied Soil Layers

Kil-Wan Ko¹ and Robert E. Kayen, M.ASCE²

Abstract: The evaluation of the excess pore water pressure ratio (r_u), the ratio of the excess pore water pressure of the soil, is a defining approach to assessing liquefaction occurrence. Rarely is r_u measured, so surficial observations of sand boils, fissures, and soil settlements have provided indirect evidence of liquefaction occurrence in case histories. Acceleration responses during undrained cyclic loadings incorporate shear strain and stress responses of the liquefied soil. Therefore, the use of acceleration responses can provide another indirect indication of liquefaction as the sudden drop in the frequency in the time–frequency domain in acceleration records. This study aimed to develop strain-based and energy-based methods for estimating the pore water pressure buildup based on the acceleration responses of liquefiable sand layers. The strain-based method linked the liquefaction-induced shear strain of the soil with r_u through the shear modulus that is a function of the effective stress. An alternative approach used an energy-based method that linked pore-pressure generation with the energy dissipated in the soil. Centrifuge model tests for the liquefaction of soil were used to develop and validate the two methods, and these were applied to a case history, the 1987 Superstition Hill earthquake at the Wildlife site, for validation. To capture the variation of r_u from its contractive to dilative responses, the amount of r_u drop was estimated based on the peak shear stress when dilation spikes occurred. For the energy-based method, the centrifuge test results were used to derive empirical relations between r_u and cumulative dissipated energy done by liquefiable soil. The estimated r_u time-histories from the established methods were consistent with the measured responses in the centrifuge tests and the case history. DOI: [10.1061/JGGEFK.GTENG-11458](https://doi.org/10.1061/JGGEFK.GTENG-11458). © 2024 American Society of Civil Engineers.

Author keywords: Soil liquefaction; 1987 Superstition Hill earthquake; Centrifuge model test; Excess pore water pressure ratio; Energy-based liquefaction evaluation.

Introduction

The Niigata earthquake (M_w , 7.5) of June 16, 1964, and the Alaska earthquake (M_w , 9.2) of March 27, 1964, have raised awareness of the severity of liquefaction consequences for infrastructure (Bartlett and Youd 1995; Ishihara and Koga 1981). Over the last six decades, reconnaissance and in situ tests of liquefaction sites subjected to earthquakes have characterized the liquefiable sites based on the empirical relations between the earthquake-induced shear stresses and in situ test indices for liquefaction resistance (Seed et al. 1985; Boulanger and Idriss 2012; Cetin et al. 2004, 2018; Kayen et al. 2013; Moss et al. 2006; Seed and Idriss 1971; Youd et al. 2001). Surficial observations such as ground fissures, sand boils, uplifting of pipelines or tanks, and so on have been used to find liquefaction occurrence at sites (Youd et al. 2001; NAS 2021), though the surficial evidence does not indicate the triggering but rather the consequence of soil liquefaction. Depending on the soil strata, surficial evidence might not manifest when liquefaction occurs at depth (Kostadinov and Yamazaki 2001; Kramer et al. 2016).

Liquefiable soil layers transfer normal stress from the soil particles onto the pore water and result in the loss of soil strength and

stiffness (Idriss and Boulanger 2008). Accordingly, the excess pore water pressure ratio ($r_u = \Delta u / \sigma'$), which is a ratio of the excess pore water pressure (Δu) to the initial effective stress of the soil (σ'), defines the triggering of soil liquefaction during earthquakes. Unfortunately, nearly all strong-motion stations have only recorded acceleration records without pore water pressure responses [e.g., K-NET (Kyoshin network), KiK-net (Kiban Kyoshin network), and Center for Engineering Strong Motion Data (CESMD)] (Haddadi et al. 2008; NIED 2019). At nearly every case history in the global databases of liquefaction performance, the defining parameter for liquefaction triggering has not been measured, and only a few cases have acceleration records on liquefying soil layers. For these records, the observation of period lengthening (frequency drop) of the soil layer indicates the triggering of liquefaction over the time–frequency domain of the acceleration time history due to the loss of soil stiffness within the liquefied soil (Kostadinov and Yamazaki 2001; Kramer et al. 2016; Manandhar et al. 2021; Unjoh et al. 2012). Although the time–frequency domain reveals the timing of liquefaction, the method is inadequate for partially liquefied soil, which does not lead to a remarkable frequency drop over the time–frequency domain response but develops excess pore water pressure by retaining some of the soil stiffness.

Previous literature introduced the use of the energy-based approaches to evaluate the liquefaction potential (Berrill and Davis 1985; Figueroa et al. 1994; Kokusho 2013, 2021; Kokusho and Tanimoto 2021; Nemat-Nasser and Shokoh 1979). The salient principle of the approach is that the required cumulative energy to develop pore pressure under the undrained condition is associated with the work done by the liquefiable sand, in that the dissipated energy can be estimated from the stress–strain hysteresis loops of the soil. Based on this principle, empirical relations between Δu and the cumulative energy from the lab tests such as cyclic triaxial and

¹Postdoctoral Researcher, Dept. of Civil and Environmental Engineering, Univ. of California, Berkeley, CA 94720. ORCID: <https://orcid.org/0000-0002-0356-072X>. Email: kwko@berkeley.edu

²Professor, Dept. of Civil and Environmental Engineering, Univ. of California, Berkeley, CA 94720 (corresponding author). Email: rkayen@berkeley.edu

Note. This manuscript was submitted on November 1, 2022; approved on February 23, 2024; published online on July 23, 2024. Discussion period open until December 23, 2024; separate discussions must be submitted for individual papers. This paper is part of the *Journal of Geotechnical and Geoenvironmental Engineering*, © ASCE, ISSN 1090-0241.

torsional shear tests were developed (Green et al. 2000; Polito et al. 2008; Selig et al. 1983; Towhata and Ishihara 1985). Egan and Rosidi (1991) and Kayen and Mitchell (1997) applied the energy-based approach to the field condition by representing the seismic loading in terms of an energy-based intensity measure such as Arias intensity. The cumulative dissipated energy of the soil incorporates the effect of the applied number of cycles, shear stress, frequency, duration, and amplitude of earthquake motion. One of the advantages of this approach therefore is that correction factors are not needed to adjust for numbers of cycles and earthquake magnitude.

Experimental results have demonstrated that the generation of excess pore water pressure is strongly related to the shear strain (γ) of the soil (Dobry et al. 1982; Idriss and Boulanger 2008). Shear modulus (G) degradation of the soil is a function of the shear strain of the soil. Effective stress changes of the soil govern the undrained cyclic response of coarse-grained material, so the reduction of effective stress due to excess pore pressure generation leads to a reduction in the shear modulus of the soil (Kramer et al. 2016). Accordingly, the time-varying shear strain of the soil during shaking can directly be used to estimate the amount of excess pore water pressure development through the time-varying shear modulus. In other words, the stress–strain responses and cumulative dissipated energy of liquefiable soil layers, estimated through the acceleration responses, can provide comprehensive insights into the behavior of liquefied soil during earthquakes. This presents a potential method of assessing the r_u buildup over time, using acceleration records under the assumption of a shear beam behavior in liquefied soil. However, this assumption simplifies the responses of multilayered soil as one-dimensional shear beam behavior without accounting for the lateral stress variations in soil during earthquakes.

The objective of this study is to explore energy-based and strain-based methods in order to estimate the time-varying r_u during shaking. First, the methodologies to obtain the cumulative energy and shear strain of the soil using acceleration responses are described. The empirical relations between r_u and cumulative dissipated energy done by the soil were developed. The developed methodologies estimated the general trend of r_u over time during shaking, but they could not track the transient reduction spikes of r_u due to the dilational behavior of the liquefied soil. Further investigation revealed that the dilation spike in the shear stress (τ) response presented a way to track the transient reduction spike on r_u over the time history. Here, the centrifuge tests from Liquefaction Experiment and Analysis Projects (LEAP) (Kutter et al. 2020) provided important experimental data to develop and validate the methods. Another centrifuge test with the multilayered soil using a real earthquake record demonstrated the applicability of the proposed methods. The applicability of the methods to the field condition was also validated by using a case history from the Wildlife site (Imperial County, California) data recorded during the Superstition Hills earthquake (November 24, 1987). Finally, this study performed sensitivity analyses of shear modulus reduction curves for strain-based estimation and effect of height of the soil layer, and it delved into the limitations of this study.

Shear Stress–Strain Behavior of Saturated Sand and Methodologies for Estimation of Excess Pore Water Pressure Ratio

Dynamic shear stress–strain response of the liquefiable soil links the acceleration responses to the time-varying r_u during shaking. Undrained cyclic soil behavior produces multiple stages of contractive and dilative behavior with fluctuations of r_u during earthquake loading, even after the soil has liquefied.

Shear Stress–Strain Response

Shear stress–strain response and effective stress change of the soil provide intuitive information about the state of the soil and whether the soil is liquefied. Laboratory tests judge the liquefaction initiation when the cyclic shear strain exceeds 3% in single amplitude in cyclic triaxial tests (Idriss and Boulanger 2008). During loading, the shear modulus varies due to repeated liquefaction and deliquification. If the effect of lateral stress variations on the soil layer is neglected, the lateral stress–strain response that the soil layer undergoes can be calculated using a one-dimensional shear beam model. Using vertically aligned accelerometers, Zeghal et al. (2018) introduced a way to calculate the shear stress–strain response using two acceleration and displacement records that are obtained by the double integration of the acceleration response.

Shear stress–strain, effective stress, and excess pore water pressure ratio enable delineation of the undrained cyclic behavior of a saturated soil layer under the dynamic loading in Fig. 1. The figure describes the responses of the soil layer at 2 m depth from a centrifuge test from Ehime 3 of the LEAP, whose experimental description will be explained in the section “Centrifuge Tests: Liquefaction Experiment and Analysis Project.” When dynamic loading applies to the saturated sand, the effective stress decreases as the shear strain and excess pore pressure develop from the initial state (a green circle in Fig. 1). The persisting dynamic loading liquefies the soil, which loses its shear stiffness and indicates a large induced shear strain with zero effective stress and $r_u = 1$ ($r_{u,max}$, which is a local maximum of r_u at that cycle, a blue circle in Fig. 1). Continued cyclic loading leads to the dilational response of the liquefied soil beyond the phase transformation line (PTL), which results in the transient decrease in r_u ($r_{u,min}$, which is a local minimum of r_u at that cycle) with increasing the effective stress (a red circle in Fig. 1). Loose sand under a large confining stress tends to deform distinctly at the beginning of a cycle, contractive behavior, and then it starts to dilate, approaching the steady state at the end (Ishihara 1993). According to the contractive and dilative behavior, there is a boundary between contractive and dilative behavior of soil, which is the PTL. At this moment, deliquification shock waves (Kutter and Wilson 1999) impose shear stress spikes on the liquefied soil in response to the temporarily increased shear stiffness of the soil. In other words, the shear stress spikes due to dilational response and the amount of sudden drop of r_u ($r_{u,max} - r_{u,min}$, which is the difference between the local maximum and minimum of r_u at a cycle) may correlate to each other, and the timing of those responses is the same [Fig. 1(d)]. The contractive and dilative responses of the liquefied soil repeatedly occur under dynamic loading. Here, methodologies are introduced to model the trend line of $r_{u,max}$ and $[r_{u,max} - r_{u,min}]$ over time based on the shear stress and strain records. The value of $r_{u,min}$ is estimated by subtracting $[r_{u,max} - r_{u,min}]$ from $r_{u,max}$.

Strain-Based r_u Estimation

The maximum shear modulus at the low-strain level (G_{max}) and G/G_{max} are a function of the effective stress in the direction of wave propagation and shear strain of the soil, respectively (Roessler 1979). The effective stress changes in accordance with the change of r_u throughout the undrained cyclic response. Accordingly, the shear modulus connects the relation between the induced shear strain and r_u of the sand. Strain-based r_u estimation requires two horizontal acceleration time histories in a vertical array, which affords time-varying strain of the soil layer sandwiched between the accelerometers, shear modulus degradation curves of the soil (G/G_{max}), and an empirical relation between $r_{u,max} - r_{u,min}$ and τ for the soil layer. A step-by-step procedure estimating the r_u over the time-history follows (Fig. 2).

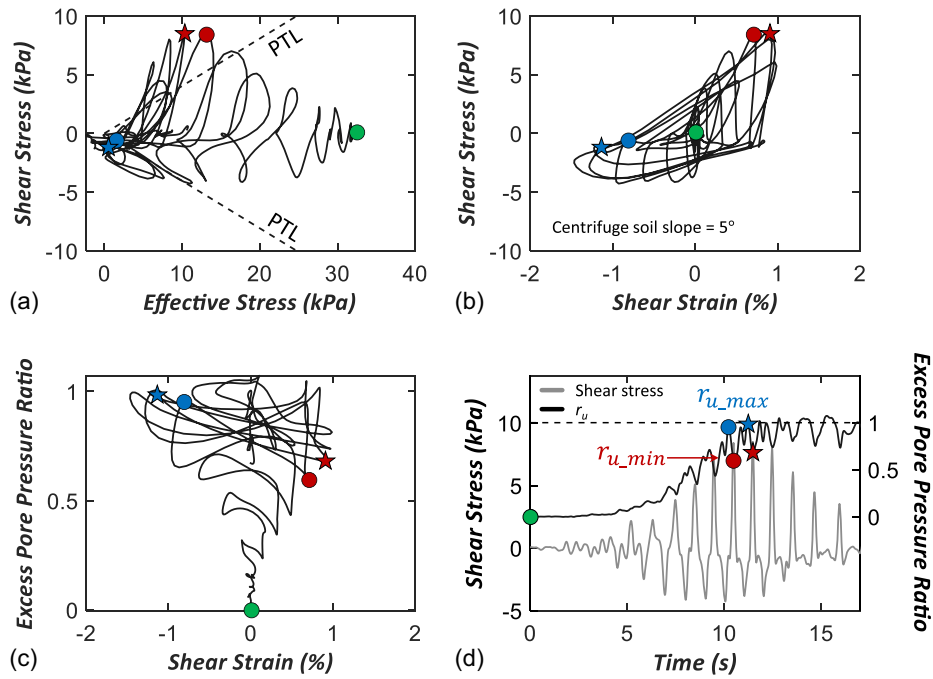


Fig. 1. Undrained cyclic responses of a saturated soil layer under the dynamic loading (the soil layer at 2 m depth from a centrifuge test of Ehime 3): (a) effective stress and shear stress responses; (b) shear strain and shear stress responses; (c) shear strain and excess pore pressure ratio; and (d) time histories of shear stress and excess pore pressure ratio.

Strain-Based Estimation

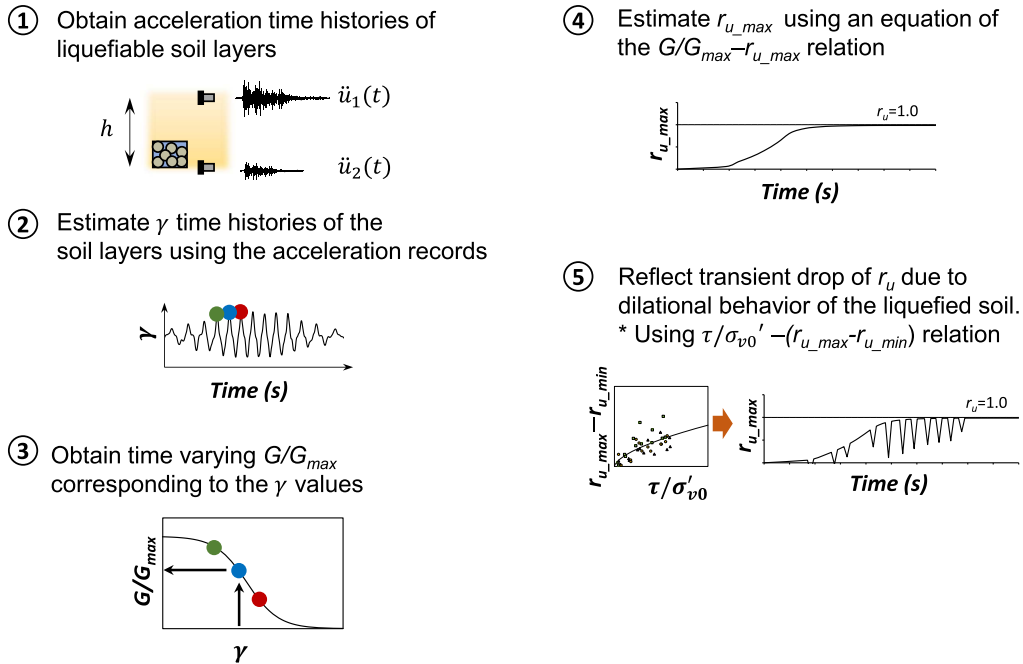


Fig. 2. Step-by-step procedure estimating the excess pore water pressure ratio using the shear strain of the soil.

1. Obtain the two horizontal acceleration time histories $[\ddot{u}_1(t)$ and $\ddot{u}_2(t)]$ installed in the target liquefiable soil layer. The distance between the vertically aligned accelerometers is h .
2. Calculate the time-varying shear strain $[\gamma(t)]$ of the soil layer using double-integrated displacement time histories $[u_1(t)$ and $u_2(t)]$ from the acceleration records, as follows:

$$\gamma(t) = \frac{u_1(t) - u_2(t)}{h} \quad (1)$$

3. Obtain time-varying $G/G_{max}(t)$ corresponding to the $\gamma(t)$ using the G/G_{max} curve of the soil layer.
4. Back-calculate $r_{u,max}$ from $G/G_{max}(t)$ using Eq. (2) from Kramer et al. (2016), as follows:

Energy-Based Estimation

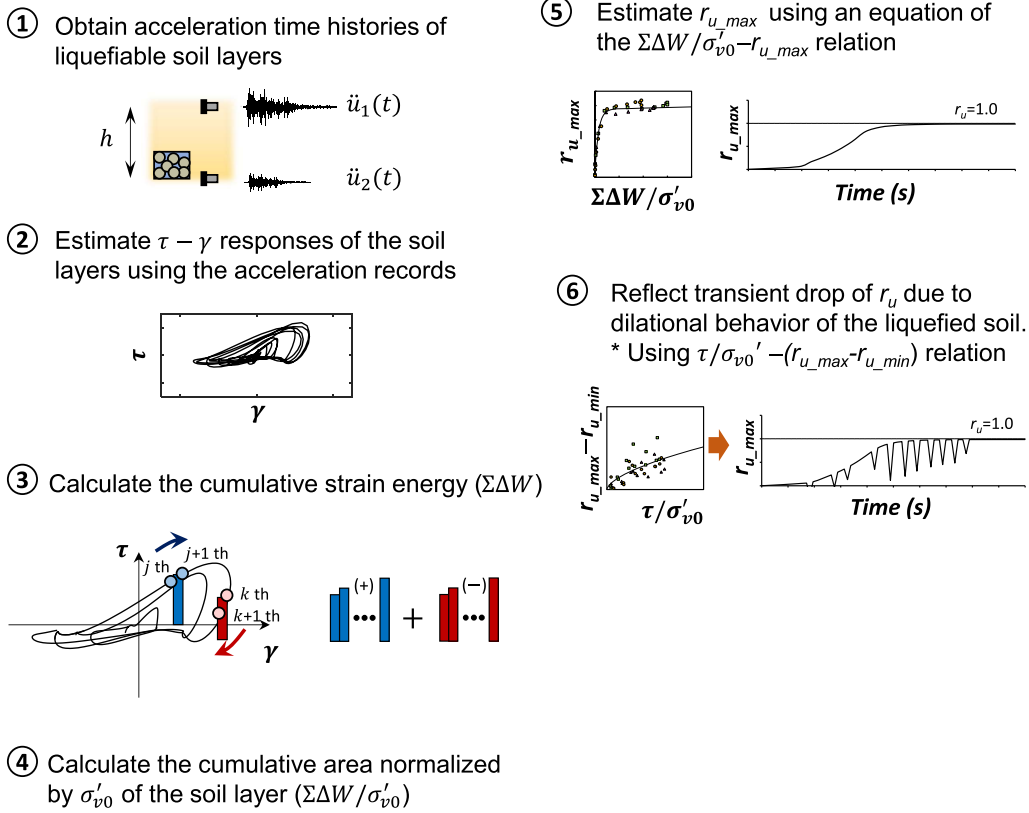


Fig. 3. Step-by-step procedure estimating the excess pore water pressure ratio using the cumulative dissipated energy of the soil.

$$G = G_0 \sqrt{\frac{\sigma'_{v0}(1 - r_u)}{P_a}} \quad (2)$$

$$r_{u_max}(t) = 1 - \frac{P_a}{\sigma'_{v0}} \left(\frac{G}{G_0} \right)^2 = 1 - \frac{P_a}{\sigma'_{v0}} \left(\frac{G}{G_{max} \left(\sqrt{\frac{P_a}{\sigma'_{v0}}} \right)} \right)^2 \quad (3)$$

$$= 1 - (G/G_{max}(t))^2$$

where P_a = atmospheric pressure; σ'_{v0} = vertical effective stress; and G_0 and V_{s0} = maximum shear modulus and shear wave velocity at an effective stress of 1 atm, respectively.

5. Subtract $r_{u_max} - r_{u_min}$, which is a function of τ/σ'_{v0} , from r_{u_max} to reflect the transient drop of r_u due to the dilational behavior of the liquefied soil. The timing of the transient drop of r_u response is consistent with that of dilational spikes in the shear stress domain. The half cycle duration of each spike pulse is 0.05 s because the minimum frequency of dilation spikes corresponds to 10 Hz (Kutter and Wilson 1999; Hutabarat and Bray 2019; Manandhar et al. 2021). However, the frequency of dilation spikes could change based on the effects of soil heterogeneity and ground motions.

Energy-Based r_u Estimation

The cyclic response of the saturated sand generates hysteresis loops whose area is associated with the dissipated energy (ΔW) by the soil. Laboratory tests from the previous literature, which studied the cyclic behavior of the saturated sand under undrained condition, corroborate the possibility of estimating r_u based on the cumulative

energy ($\Sigma \Delta W$) calculated by the shear stress–strain response of the soil (Kokusho 2013, 2021; Kokusho and Tanimoto 2021). The essential information for energy-based r_u estimation comprises the shear stress–strain cyclic response of the soil layer obtained from vertically aligned acceleration records, the empirical relation between cumulative energy and r_{u_max} , the soil density (ρ), and an empirical relation between $r_{u_max} - r_{u_min}$ and τ for the soil layer. A step-by-step procedure estimating r_u over the time history follows (Fig. 3).

1. Follow the Step 1 from the strain-based method.
2. Calculate the shear stress (τ) and strain (γ) of the soil layer using acceleration records (Zeghal et al. 2018). The shear stress (τ_i) at level h_i of the i th accelerometer is calculated, as follows:

$$\tau_i(t) = \tau_{i-1}(t) + \rho \frac{\ddot{u}_{i-1} + \ddot{u}_i}{2} \Delta h_{i-1}, \quad i = 2, 3, \dots \quad (4)$$

where Δh_{i-1} = distance between the vertically aligned accelerometers measuring $\ddot{u}_i(t)$ and $\ddot{u}_{i-1}(t)$; and τ at the soil surface = 0. Shear stress ($\tau_{i-1/2}$) at the midpoint between the i th and $i-1$ th accelerometers representing the shear stress of the layer is estimated through linear interpolation as

$$\tau_{i-1/2}(t) = \tau_{i-1}(t) + \rho \frac{3\ddot{u}_{i-1} + \ddot{u}_i}{8} \Delta h_{i-1}, \quad i = 2, 3, \dots \quad (5)$$

For the energy-based method, $\tau_{i-1/2}(t)$ and γ from Eq. (1) are used to obtain the hysteresis loops.

3. Calculate the change in strain energy ΔW over time using hysteresis loops of τ and γ . The trapezoidal rule calculates the cumulative strain energy $\Sigma \Delta W$ as follows (Polito et al. 2008):

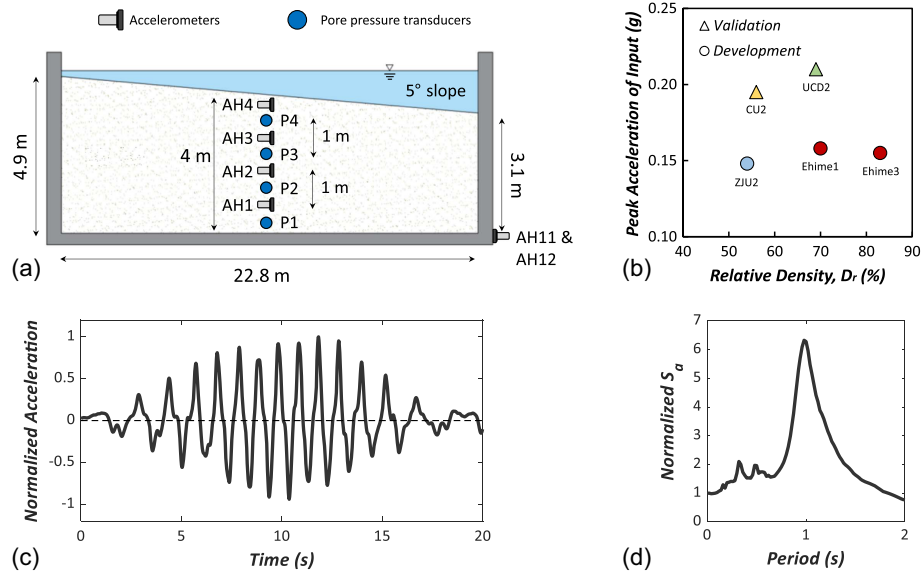


Fig. 4. Centrifuge model tests for the Liquefaction Experiment and Analysis Projects (LEAP-UCD-2017): (a) sectional view of the centrifuge test setup in prototype scale; (b) peak acceleration of input and relative density of the test data used for this study from the LEAP; (c) normalized acceleration time history of the input motion; and (d) normalized response spectrum of the input motion.

$$\tau_{avg,j} = \begin{cases} \frac{|\tau_{j+1} + \tau_j|}{2}, & \tau_{j+1} \cdot \tau_j \geq 0 \\ \frac{\tau_{j+1}^2 + \tau_j^2}{2 \cdot |\tau_{j+1} - \tau_j|}, & \tau_{j+1} \cdot \tau_j < 0 \end{cases} \quad (6)$$

$$\Sigma \Delta W = \sum_{j=1}^{n-1} \tau_{avg,j} (\gamma_{j+1} - \gamma_j) \quad (7)$$

where τ_j and τ_{j+1} = shear stress at each time step of j and $j + 1$, respectively; γ_j and γ_{j+1} = shear strain at each time step of j and $j + 1$, respectively; and $\Sigma \Delta W$ = cumulative strain energy dissipated by soil per unit volume, and its unit is N/m^2 . Applied and recovered strain energy during the soil's cyclic behavior are automatically inclusive to Eq. (6) due to the sign changes of τ and γ during earthquakes (Millen et al. 2021).

4. Calculate the cumulative dissipated energy normalized by σ'_{v0} of the target soil layer ($\Sigma \Delta W / \sigma'_{v0}$).
5. Estimate $r_{u,max}$ using an empirical equation related to the $\Sigma \Delta W / \sigma'_{v0}$ and $r_{u,max}$. The empirical equation is formed as follows:

$$r_{u,max} = \frac{\Sigma \Delta W / \sigma'_{v0}}{\Sigma \Delta W / \sigma'_{v0} + a} \quad (8)$$

where a = empirical coefficient. The specific description of the equation will be discussed in the section "Development of Empirical Equations for the Methods to Estimate r_u ."

6. Follow Step 7 from the strain-based method.

Centrifuge Tests: Liquefaction Experiment and Analysis Projects

LEAP was a collaborative research project with the primary objective of producing high-quality centrifuge data for validating and calibrating constitutive models for numerical simulations (Kutter et al. 2020). The project focused on producing reliable centrifuge data for liquefaction problems from nine centrifuge research centers using a common controlled ground model, physical properties of

the soil, and input motion. This study employed LEAP-UCD-2017 data, in which nine different centrifuge centers around the world participated for investigating dynamic responses of mildly sloping liquefiable soils [Fig. 4(a)]. The employed centrifuge data were used to develop empirical equations for the $\Sigma \Delta W / \sigma'_{v0}$ and $r_{u,max}$ relation and the τ / σ'_{v0} and $r_{u,max} - r_{u,min}$ relation.

Centrifuge Testing Model

The participating centrifuge centers applied different centrifugal accelerations to the testing model to simulate the same size of the model ground at prototype scale using different sizes of the model boxes at each center. This study expresses the testing results and model description in the prototype scale by applying scaling laws (Schofield 1980).

The gently sloping ground of 5° was reconstituted by a pluviation method using Ottawa F-65 sand (Table 1) [Fig. 4(a)]. For the simulation of the flow of pore water in the prototype scale, a viscous fluid comprising methylcellulose and water was used to saturate the model ground. In accordance with the scaling law, the target viscosity of the fluid was decided (Garnier et al. 2007). All the centers followed the guidelines for the saturation process provided by LEAP-UCD-2017. A vertical array of accelerometers (AH1–AH4) with a vertical spacing of 1 m was installed at the center of the model to measure the horizontal acceleration of the ground. A vertical array of pore pressure transducers (P1–P4) was located beside the accelerometers. The distance between each accelerometer and pore pressure transducer was 0.5 m. The specific

Table 1. Ottawa F-65 sand properties

Soil model properties	Value
Specific gravity, G_s	2.65
Maximum void ratio, e_{max}	0.78
Minimum void ratio, e_{min}	0.51
Mean grain size, D_{50} (mm)	0.2
Coefficient of uniformity, C_u	1.728
Coefficient of curvature, C_c	0.947

Table 2. Summary of the centrifuge tests for each facility

Facility	Testing model	G-level	Density (kg/m ³)	Relative density (%)	Peak input acceleration (g)	Purpose of using data	Pore water pressure transducers		
							Sensors	Depth (m)	Vertical effective stress, σ'_{v0} (kPa)
Cambridge	CU2	40	1,606	56	0.195	Validation	P1	3.88	38.56
							P2	2.96	29.42
							P3	2.05	20.39
							P4	0.97	9.66
Ehime	Ehime 1	40	1,649	70	0.158	Development	P1	4.00	40.70
							P2	3.12	31.74
							P3	2.24	22.79
							P4	1.52	15.46
	Ehime 3	40	1,693	83	0.155	Development	P1	4.00	41.61
							P2	3.12	32.46
							P3	2.28	23.72
							P4	1.40	14.56
University of California, Davis	UCD2	43.75	1,648	70	0.21	Validation	P1	3.85	39.07
							P2	3.00	30.45
							P3	2.00	20.32
							P4	1.00	10.14
Zhejiang	ZJU2	30	1,599	55	0.148	Development	P1	3.85	38.13
							P2	3.00	29.69
							P3	2.00	19.77
							P4	0.99	9.85

descriptions of the centrifuge tests and model for each center are provided in Kutter et al. (2020).

The test matrix of LEAP-UCD-2017 consists of the relative density of the ground model and the peak acceleration of an input motion [Fig. 4(b)]. Here, to develop and validate the methods, this study selected the test data from the University of Cambridge; Ehime University; University of California, Davis; and Zhejiang University, whose test results were labeled CU2, Ehime 1 and 3, UCD2, and ZJU2, respectively (Table 2). Three test results (Ehime 1, Ehime 3, and ZJU2) having a different relative density of the soil under similar peak acceleration of the input motion around 0.15 g were used to develop the empirical equations. Two test results (CU2 and UCD2) were used to validate the methods. The relative density of CU2 and UCD2 is similar to that of ZJU2 and Ehime 1, respectively, but with different peak accelerations of the input. Hence, the empirical equations for the developed methods from ZJU2 and Ehime 1 facilitated estimating r_u using acceleration records and validating the results from CU2 and UCD2, respectively. In order to obtain r_u , centrifuge tests estimated the vertical effective stress (σ'_{v0}) at the depth where the pore pressure transducers (P1–P4) were installed. As an example, if the depth of P1 is z_1 from the soil surface, σ'_{v0} at z_1 is computed as follows:

$$\sigma'_{v0} = \gamma' \times z_1 = (\gamma_{sat} - \gamma_w) \times z_1 = \left(\frac{(G_s + e)\gamma_w}{1 + e} - \gamma_w \right) \times z_1 \quad (9)$$

where γ' = submerged unit weight of soil; γ_{sat} = saturated unit weight of soil; γ_w = unit weight of soil, 9.81 kN/m³; G_s = specific gravity of the soil; and e = void ratio. The void ratio can be calculated by using the relative density of soil (D_r), maximum void ratio (e_{max}), and minimum void ratio (e_{min}). The obtained σ'_{v0} values for each pore pressure transducer are summarized in Table 2.

LEAP-UCD-2017 guided the tests to apply a smooth ramped sine wave to the model as the first destructive motion [Fig. 4(c)]. The duration and frequency of the input motion were the same for each test, but the peak acceleration of the input differed. The duration of the signal was around 20 s. The input motion was sine 1 Hz [Fig. 4(d)], which could exclude the frequency effect because

the fundamental frequency of the model was over 7 Hz, significantly higher than that of the input motion (Manandhar et al. 2021). A fifth-order Butterworth band-pass filter with corner frequencies of 0.1–20 Hz was applied to the acceleration records. Baseline correction then offset the measured acceleration time histories for each centrifuge test.

A Representative Centrifuge Test Result (Ehime 1)

A representative centrifuge test result from Ehime 1 is depicted in Fig. 5. The acceleration amplitude increased as the depth decreased due to the site amplification. In the acceleration responses of the depth of 1.5 and 0.5 m, the acceleration records repeated the amplitude close to zero (flat response) and spikes (dilation spikes). This phenomenon is attributed to the contractive (loss of the effective stress and shear stiffness of the soil) and dilative behavior (a sudden increase of the shear stiffness of the soil) of the undrained soil under earthquake loadings, and the phenomenon is more apparent in the soil layer close to the surface. The shear stress–strain curves represent the dynamic behavior of the soil layer between the installed depths of two vertical accelerometers. According to the liquefaction triggering criterion for laboratory tests (e.g., cyclic triaxial and cyclic simple shear tests), the strain level for every depth did not exceed 3%, which indicates that the soil layer did not liquefy. However, the strain level decreased as the depth of the soil decreased due to the base-isolation effect (Kokusho 2014). The liquefaction triggering criterion based on the strain level, therefore, was not appropriate for the centrifuge tests. The soil liquefaction occurrence induced a significant strain level at a depth of 3 m that became a boundary between the liquefied and nonliquefied soil layers. The G/G_{max} curve exhibited shear modulus reduction according to the shear strain of Ottawa F-65 (Ramirez et al. 2018). The G/G_{max} value according to the shear strain level at a certain time was used to estimate r_u from the strain-based method. At depths of 3, 2, and 1 m where the pore water pressure transducers were installed, the pore pressure responses reached the point $r_u = 1$, which implies the soil layers were fully liquefied at that depth.

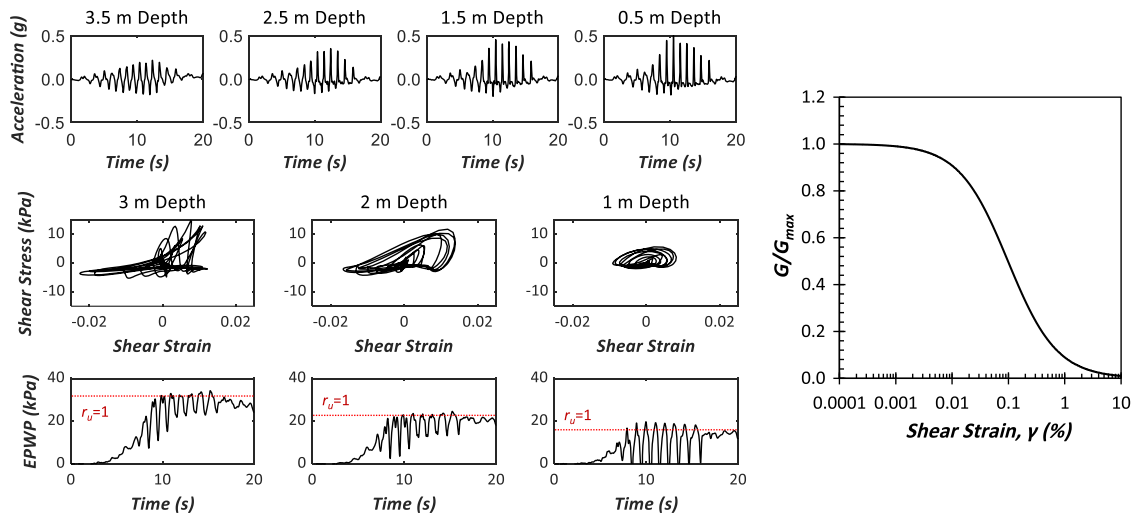


Fig. 5. Representative centrifuge test result (Ehime 1): acceleration time histories, shear stress–strain responses, pore water pressure responses, and G/G_{\max} curve (Ottawa F-65).

Table 3. Coefficients, standard deviation (s), and R -squared (R^2) of empirical equations [Eqs. (8) and (10)]

Testing model	Relative density (%)	$r_{u_{\max}} = \frac{\Sigma\Delta W/\sigma'_{v0}}{\Sigma\Delta W/\sigma'_{v0} + a}$			$\ln(r_{u_{\max}} - r_{u_{\min}}) = b \times \ln(\tau/\sigma'_{v0}) + c$			
		a	s	R^2	b	c	s	R^2
Ehime 1	70	3.22×10^{-4}	0.06	0.98	0.68	-0.04	0.14	0.63
Ehime 3	83	3.89×10^{-4}	0.05	0.98	0.61	-0.35	0.11	0.48
ZJU2	55	2.57×10^{-4}	0.13	0.87	0.74	0.35	0.15	0.46

Development of Empirical Equations for the Methods to Estimate r_u

The empirical equations of $\Sigma\Delta W/\sigma'_{v0}$ and $r_{u_{\max}}$ and $r_{u_{\max}} - r_{u_{\min}}$ and τ/σ'_{v0} are necessary for the energy-based, strain-based methods and featuring the dilative behavior of the liquefied soil. For developing the empirical equations, the stress–strain hysteresis loops were divided into discrete cycles based on the moment when the shear stresses were equal to zero. After this, the cumulative energy $\Sigma\Delta W$ was estimated by adding the calculated areas of the discrete cycles, and $r_{u_{\max}}$ and the peak τ of the discrete cycle were decided. The process was applied to each depth of the soil layer, and $\Sigma\Delta W$ was normalized by the σ'_{v0} at that soil layer. As shown in Fig. 1, saturated sand demonstrates contractive and dilative behavior during cyclic loadings, which results in a local maximum ($r_{u_{\max}}$) and minimum ($r_{u_{\min}}$) in each cycle. The objective of developing an empirical relation between $r_{u_{\max}} - r_{u_{\min}}$ and τ/σ'_{v0} was to capture the dilative and contractive behavior of the soil for each cycle. For the empirical relation between $r_{u_{\max}} - r_{u_{\min}}$ and τ/σ'_{v0} , the peak shear stress normalized by σ'_{v0} of the soil layer and the local decrease in r_u for each cycle $r_{u_{\max}} - r_{u_{\min}}$ were obtained based on each discrete cycle.

The empirical equation of $r_{u_{\max}}$ and $\Sigma\Delta W/\sigma'_{v0}$ should satisfy the boundary conditions that the excess pore water pressure is equal to 0 when $\Sigma\Delta W/\sigma'_{v0} = 0$. Accordingly, the empirical equation was formed as Eq. (8). Table 3 summarizes the coefficient, standard deviation (s), and R -squared (R^2) for each testing model. Fig. 6 demonstrates $r_{u_{\max}}$ and $\Sigma\Delta W/\sigma'_{v0}$ of each test for developing empirical equations. The value of $r_{u_{\max}}$ increased with $\Sigma\Delta W/\sigma'_{v0}$ for all the testing models (Fig. 6). $\Sigma\Delta W/\sigma'_{v0}$ varied in accordance with the relative density of the soil. The higher the relative density of the soil, the more energy is required to be liquefied, and this is

consistent with the results from the laboratory tests (Kokusho 2013). The Ottawa sand showed that a $\Sigma\Delta W/\sigma'_{v0}$ of 0.002 developed an excess pore water pressure ratio of 0.8, but the required $\Sigma\Delta W/\sigma'_{v0}$ to develop an r_u of 0.8 depends on soil properties.

The empirical equations for $r_{u_{\max}} - r_{u_{\min}}$ and τ/σ'_{v0} were obtained by linear regression in logarithmic scale, as follows:

$$\ln(r_{u_{\max}} - r_{u_{\min}}) = b \times \ln(\tau/\sigma'_{v0}) + c \quad (10)$$

where b and c = empirical coefficients; and Table 3 summarizes the coefficients, standard deviation, and R -squared for each testing model. As shown in Fig. 6, the lower the relative density of the soil, the higher the transient drop of the excess pore water pressure ($r_{u_{\max}} - r_{u_{\min}}$) due to the dilative behavior exhibited. This implies that after soil loses the effective stress due to contractive behavior under the cyclic loading, the loose soil recovers more effective stress than the dense soil when the soil tends to be dilative beyond the quasi-steady state line (phase transformation line).

Application of the Methods to Centrifuge Test Model

The developed empirical equations were used to test the applicability of the methods estimating time-varying excess pore water pressure ratio (Fig. 7). Measured r_u responses from the three testing models creating the empirical equations were compared with estimated r_u responses from the methods. In general, the estimated r_u responses were consistent with the measured r_u . The methods capture the timing of the dilation behavior of the soil in r_u , but the amplitude of the r_u drop slightly differs. However, both methods could not capture the dissipation of the excess pore water pressure. For example, the estimated r_u responses did not reflect the

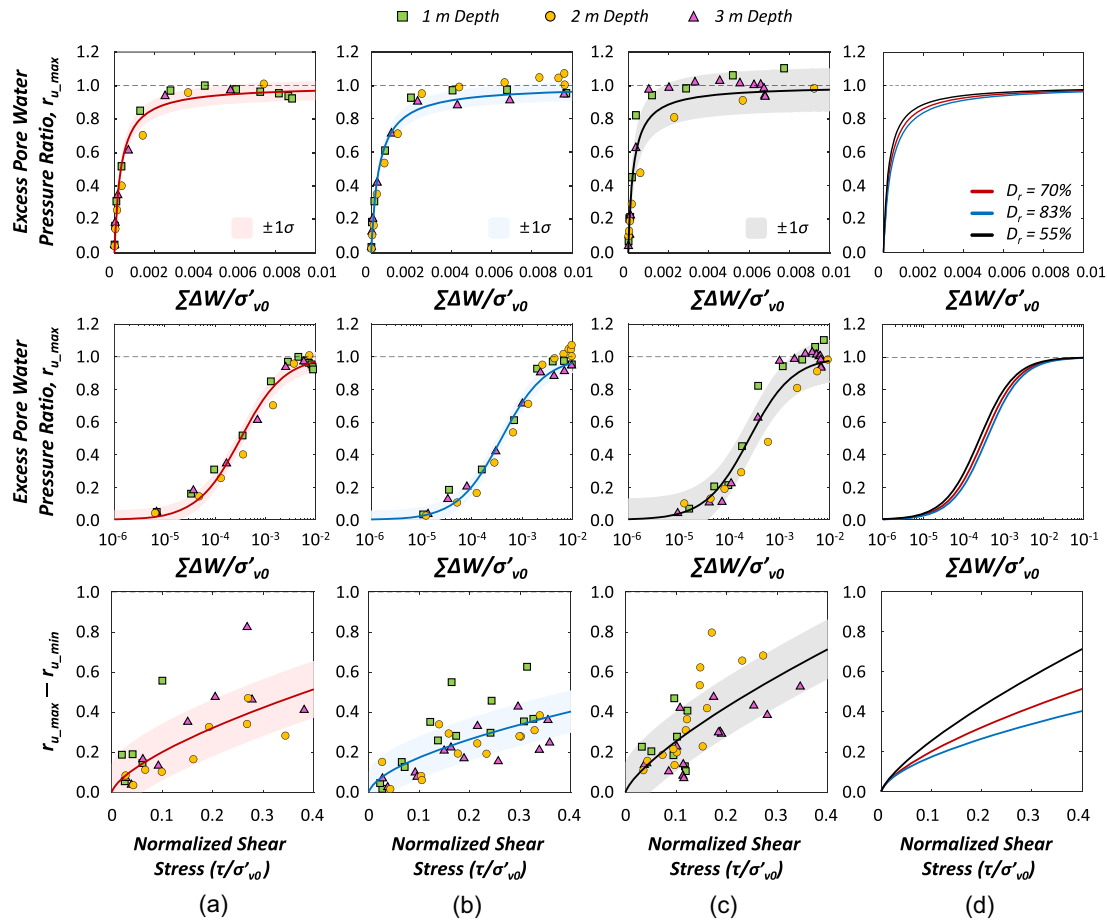


Fig. 6. Empirical equations developed from Ehime 1, Ehime 3, and ZJU2 for the strain-based and energy-based methods: excess pore water pressure ratio ($r_{u,max}$) with normalized cumulative energy ($\Sigma\Delta W/\sigma'_{v0}$) in linear scale and semi-logarithmic scale, and $r_{u,max} - r_{u,min}$ with normalized shear stress (τ/σ'_{v0}): (a) Ehime 1; (b) Ehime 3; (c) ZJU2; and (d) fitting curve.

dissipation, such as after 16 s in the depth of the 2-m and 3-m soil layers from Ehime 3 [Fig. 6(b)]. For the energy-based method, the area of the stress–strain responses is the cumulative sum of the dissipated energy with time so that the energy cannot account for the dissipation of r_u after the end of the shaking. The strain-based method generally overestimated r_u , whereas the timing of liquefaction triggering ($r_u = 1$) was comparable to that obtained from measured responses and energy-based estimation. This is attributed to the fact that G/G_{max} sensitively decreased within lower strain levels. According to the G/G_{max} of Ottawa F-65 (Fig. 5), the shear modulus value reduced by half at 0.1% shear strain from its initial value, but the shear modulus only reached 8% of its maximum value at 1% shear strain. The selection of G/G_{max} curve significantly affected the estimated r_u by the strain-based method. Therefore, the sensitivity analysis of different G/G_{max} curves for the strain-based method will be discussed in the section “Discussion and Limitations.”

Validation of the Methodologies Using Centrifuge Test Results and Case History

Validation with Centrifuge Tests from LEAP

The developed empirical equations are a function of the relative density of the soil. Therefore, the centrifuge testing models with the

same relative density but different peak accelerations of the input were selected for validation. ZJU2 ($D_r = 55\%$) and Ehime 1 ($D_r = 70\%$) provided the relations between the $\Sigma\Delta W/\sigma'_{v0}$ and $r_{u,max}$ and τ/σ'_{v0} and $r_{u,max} - r_{u,min}$ for the blind validation of CU2 ($D_r = 56\%$) and UCD2 ($D_r = 70\%$).

The estimated r_u responses from the methods were comparable with the measured responses (Fig. 8). As previously discussed, the initial r_u generation from the strain-based method led the energy-based method. For the results from CU2, both methods manifested r_u generation earlier than the measured responses. In the results of UCD2, the r_u responses from the energy-based method replicated the trend of measured r_u responses, whereas the timing of the r_u generation from the strain-based method was slightly faster than the measured responses.

Validation with the Centrifuge Test from Hayden et al. (2015)

Centrifuge Test

The LEAP tests applied only sinusoidal waves to the mildly sloping ground. In order to validate the empirical relations developed from Eqs. (8) and (10), another centrifuge test was used (Hayden et al. 2015). The original objective of this test was to examine structure–soil–structure interaction during liquefaction. This study used test T4.6–40 from Hayden et al. (2015) with a centrifugal

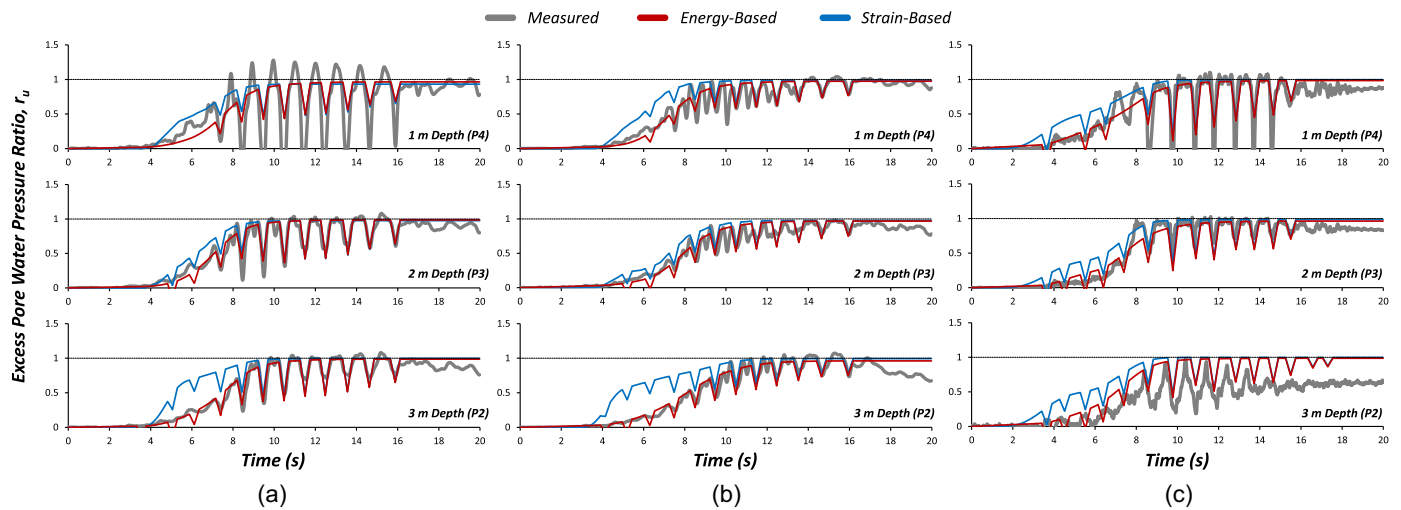


Fig. 7. Application of the strain-based and energy-based methods to centrifuge test models for estimating time-varying excess pore water pressure ratio under the dynamic loading: (a) Ehime 1; (b) Ehime 3; and (c) ZJU2.

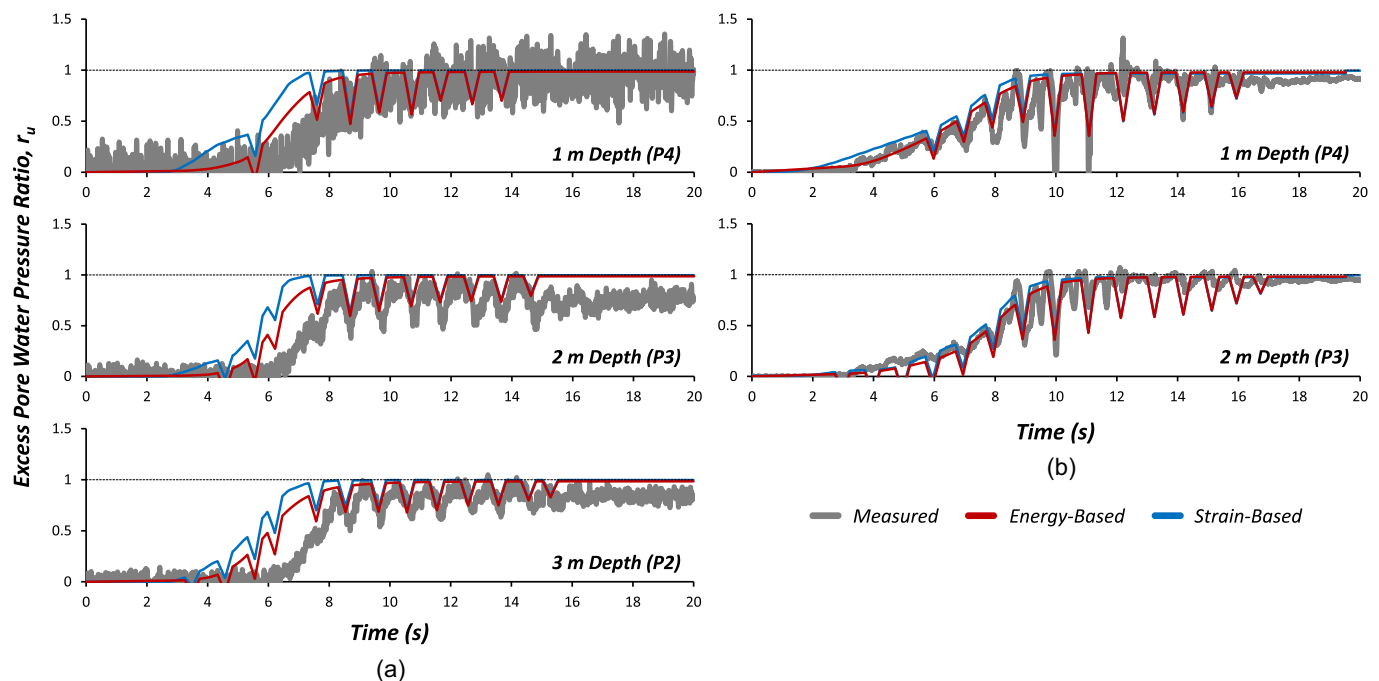


Fig. 8. Comparison between measured and estimated the excess pore water pressure ratio from the strain-based and energy-based methods: (a) CU2; and (b) UCD2.

acceleration of 55 g-level. Centrifuge data were extracted from Hayden et al. (2013) on DESIGNSAFE, and a detailed description of the test can be found in Hayden et al. (2015).

The soil model [Fig. 9(a)] consisted of 1.7-m-thick layer of dense Monterey 0/30 sand ($G_s = 2.64$, $e_{\max} = 0.54$, $e_{\min} = 0.84$, $D_{50} = 0.40$ mm) with D_r of 85%, 4.6-m-thick layer of loose Nevada sand ($G_s = 2.67$, $e_{\max} = 0.78$, $e_{\min} = 0.52$, $D_{50} = 0.14$ mm) with D_r of 40%, and 19.3-m-thick layer of dense Nevada sand with D_r of 90%. The soil was saturated with a methylcellulose-water solution with a viscosity 21 times that of water, and the water table depth was 0.2 m below the ground surface. The loose Nevada sand was highly susceptible to liquefaction during earthquakes. This study employed four accelerometers: one (Acc 3) was installed in the Monterey sand, whereas the others (Acc 71, 70, 69) were

installed in the loose Nevada sand. Additionally, two pore water pressure transducers (P37, P36) were located beside the accelerometers in the loose Nevada sand. Although these sensors were not positioned at a sufficient distance from the foundation–structure model to qualify as sensors measuring free-field responses, these sensors in a vertical array were used to validate the strain-based and energy-based methods [Fig. 9(a)]. The depth of each sensor below the ground surface was as follows: Acc 3 = 0.3 m, Acc 71 = 2.1 m, Acc 70 = 3.6 m, Acc 69 = 6.0 m, P37 = 2.2 m, and P36 = 3.8 m.

Acceleration and Pore Water Pressure Responses

This test applied a scaled version of recorded motion in the Port Island down-hole array at a depth of 83 m during the 1995 M_w 6.9

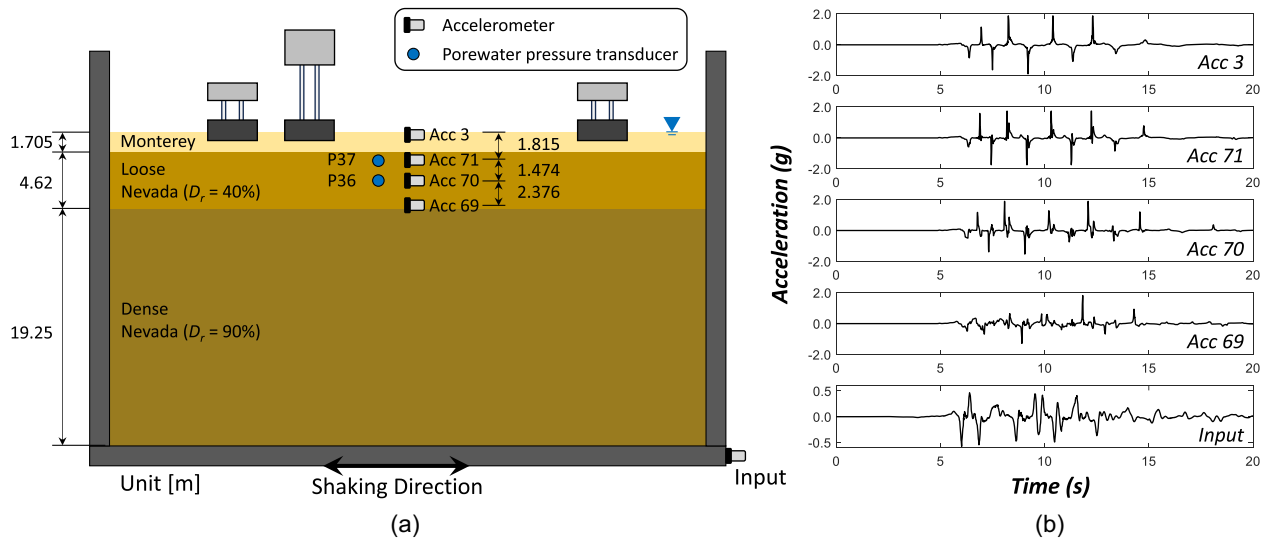


Fig. 9. Centrifuge model test from Hayden et al. (2015): (a) sectional view of the centrifuge test setup in prototype scale; and (b) acceleration time histories in a free-field vertical array.

Kobe, Japan, earthquake. The peak acceleration of input was 0.58 g [Fig. 9(b)]. As the depth decreased, the acceleration responses revealed high-frequency dilation spikes associated with the deliquification shock waves, as well as flat responses due to site softening. These observations imply liquefaction triggering in the loose Nevada sand layer.

P37 and P36 were situated between Acc 3–Acc 70 and Acc 71–Acc 69, respectively, so the strain-based and energy-based methods used pairs of Acc 3–Acc 70 and Acc 71–Acc 69 to estimate the pore water pressure responses of P37 and P36, respectively. The strain-based method employed the G/G_{max} curve of Ottawa F-65 sand, as shown in Fig. 5, and the energy-based method used the relation of $r_{u,max}$ and $\Sigma\Delta W/\sigma'_{v0}$ corresponding to a D_r of 50%, which closely matched the condition of the loose Nevada sand. Both methods also used the relation of $r_{u,max} - r_{u,min}$ and τ/σ'_{v0}

corresponding to a D_r of 50% to account for the dilation behavior of soil.

Both methods well estimated the pore water pressure responses during the earthquake (Fig. 10). The energy-based method effectively estimated the buildup of r_u whereas the strain-based method demonstrated an earlier buildup of r_u . This phenomenon arose because the energy-based method considered the stress and strain of the soil, which are affected by liquefaction, whereas the strain-based method relied solely on the strain. Furthermore, the estimated r_u from the energy-based method converged to a value less than 1, which can be attributed to the relation between $r_{u,max}$ and $\Sigma\Delta W/\sigma'_{v0}$. Although this relation represents the general behavior of soil in terms of cumulative dissipated energy, it is important to note that each soil type possesses a distinct empirical relation.

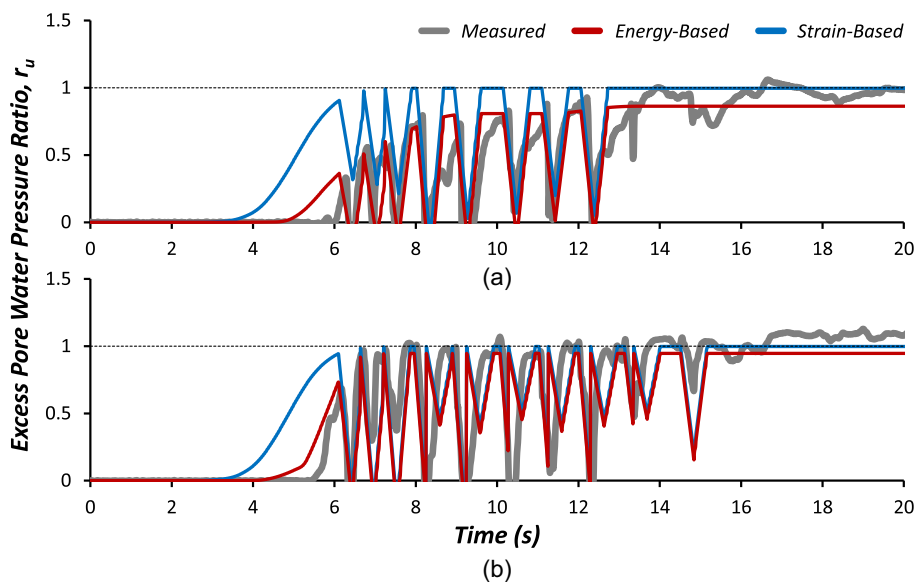


Fig. 10. Comparison of excess pore water pressure ratio between the measured and estimated responses: (a) 2.2 m depth (P37); and (b) 3.8 m depth (P36).

**Validation with a Liquefaction Field Case History:
1987 M_w 6.6 Superstition Hills, California,
Earthquake Recorded at the Wildlife Site**

Wildlife Site

The Wildlife Liquefaction Array (WLA) test site is a ground motion monitoring and liquefaction research site in California's Imperial Valley. After the initial instrumentation in 1982 by the United States Geological Survey, the Network for Earthquake Engineering Simulation (NEES) at University of California, Santa Barbara, has operated the station with a station ID of WLA (NEES@UCSB, <http://nees.ucsb.edu/data-portal>). The Wildlife site consists of layers with silt to clayey silt (depth of 0–2.5 m), silty sand to sandy silt (depth of 2.5–6.5 m), and silty clay (depth of 6.5–11.2 m) [Fig. 11(a)]. Two accelerometers and five pore pressure transducers were installed in the site. One accelerometer recorded acceleration responses of the free-field soil surface, and another accelerometer was installed in the silty clay layer with a depth of 7.5 m. Five pore pressure transducers were installed in the silty sand layer. Because the silty sand layer (depth of 2–7 m) is a highly liquefiable layer due to a shallow water table at around 1.2 m depth (Chandra et al. 2015), a transducer located at a depth of 2.9 m was used for this study. The shear stress–strain response estimated from the accelerometers represents the soil response at a depth of 3.75 m, which is the average depth of two accelerometers. The dry unit weight and shear wave velocity of the silty sand layer were 17.3 kN/m³ and 140 m/s, respectively (Youd and Carter 2005).

Previous literature (Haag and Stokoe 1985; Zeghal and Elgamal 1994; Steidl and Hegarty 2017) investigated the nonlinear shear modulus reduction (G/G_{max}) curves of the liquefiable silty sand layer [Fig. 11(b)]. Haag and Stokoe (1985) conducted resonant column tests for the upper liquefiable layer (depth of 3.26 m) by varying the confining stress with 55, 110, 220 kPa, and they provided an upper and lower bound of the G/G_{max} curves. Steidl and Hegarty (2017) calculated the shear wave velocity using classical methods, such as cross-correlation techniques using the vertical propagation of shear waves across sensors in the arrays. Zeghal and Elgamal (1994) obtained the curve from the shear stress–strain responses estimated from the accelerometers during the Superstition Hills earthquake. For the strain-based method, this study selected a G/G_{max} curve from Zeghal and Elgamal (1994), which represents the G/G_{max} curve located between the other curves.

1987 Superstition Hills Earthquake: Acceleration and Pore Water Pressure Responses

Instrumental evidence of liquefaction from the pore pressure transducers was observed during the 1987 M_w 6.6 Superstition Hills earthquake. Four pore water pressure transducers installed in the silty sand layer revealed r_u larger than 0.8 during the shaking, which directly disclosed the liquefaction occurrence at the site (Zeghal and Elgamal 1994).

Accelerometers at the soil surface and a depth of 7.5 m measured the acceleration responses in the N–S and E–W directions during the Superstition Hills earthquake [Fig. 12(a)]. Peak ground accelerations (PGAs) at a depth of 7.5 m were 0.17 g and 0.11 g in the N–S and E–W directions, respectively. Site amplification amplified acceleration responses at the soil surface so that PGAs at the soil surface were 0.21 and 0.14 g in the N–S and E–W directions. After around 25 s, acceleration responses at the soil surface manifested dilation spikes due to the dilation behavior of the soil. Stockwell transform in the time–frequency domain demonstrated frequency changes of the soil during the shaking [Fig. 12(b)]. From the beginning of the shaking to 20 s, the time–frequency response in the N–S direction had a large amount of energy around 4 Hz, which is associated with the site period. However, after 20 s, the frequency suddenly decreased to less than 1 Hz, which is the period elongation due to site softening by liquefaction (Kramer et al. 2016). The soil response in the E–W direction exhibited a similar trend to that in the N–S direction. In contrast to the N–S direction, the frequency gradually decreased from around 15 to 25 s.

The $\Sigma\Delta W/\sigma'_{v0}$ and $r_{u,max}$ relation of the Yatesville sand was used to estimate the r_u response based on the energy-based method (Green et al. 2000). The particle size distribution of the Yatesville sand (Polito and Martin 2001) was consistent with that of the silty sand at the Wildlife site (El-Sekelly et al. 2017). The empirical coefficient a was 0.0055 for the fitting curve [Eq. (8)] of the $\Sigma\Delta W/\sigma'_{v0}$ and $r_{u,max}$ relation of the Yatesville sand.

The measured pore water pressure ratio recorded at the pore water pressure (PWP) sensor buried at a depth of 2.9 m (about 1 m vertically distant from the centroid of the accelerometers) indicated the soil liquefaction occurred at approximately 35 s (Fig. 13). The energy-based and strain-based methods refer to liquefaction at the centroid. The timing of liquefaction initiation in the N–S direction was around 20 s in both estimation methods, which is consistent with that from the time–frequency response. In the E–W direction, both methods revealed that the site was liquefied at 25 s, which is the

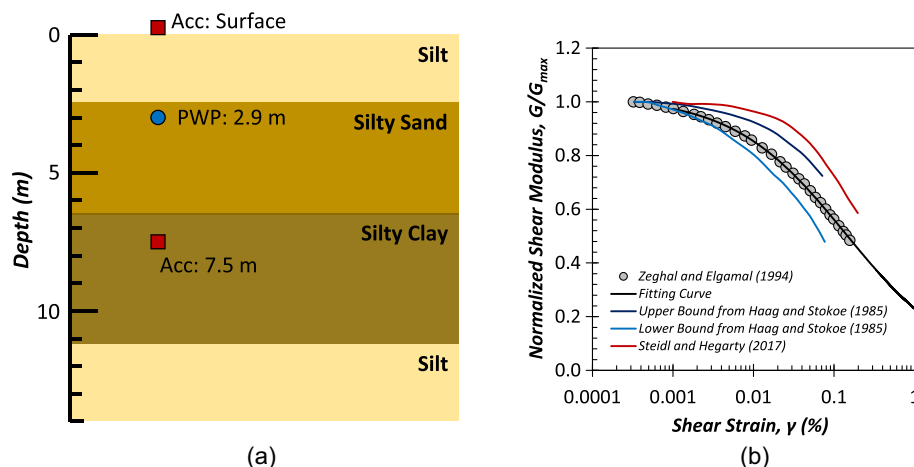


Fig. 11. Wildlife site: (a) soil strata and instrumentation; and (b) shear modulus reduction curves for the silty sand layer (depth of 2.8–6.8 m).

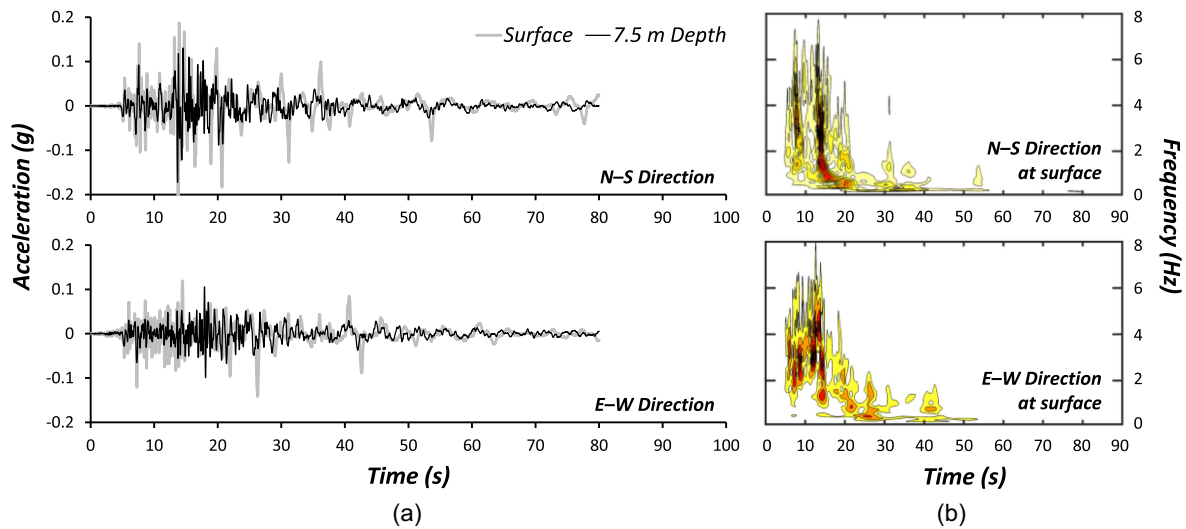


Fig. 12. Soil responses during the 1987 Superstition Hills earthquake at the Wildlife site: (a) acceleration time histories at the soil surface and a depth of 7.5 m in the N–S and E–W directions; and (b) Stockwell transform at the soil surface in the N–S and E–W directions.

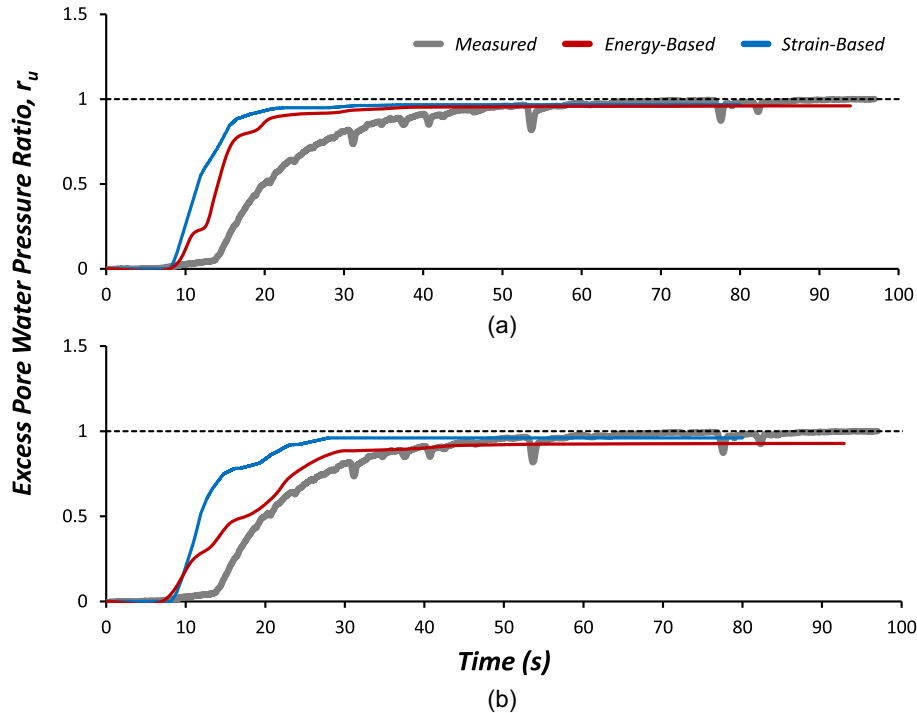


Fig. 13. Comparison of excess pore water pressure ratio at a depth of 2.9 m between the measured response and estimated responses: (a) N–S direction; and (b) E–W direction. The maximum of r_u at a depth of 2.9 m was recorded larger than 1, presumably due to underestimation of the effective stress derived from Zeghal and Elgamal (1994). Hence, the measured r_u response has been intentionally modified to satisfy $r_u = 1$ when it reaches maximum value during the shaking.

same as in the Stockwell transform. When saturated soil is under shaking, the excess pore water pressure develops within the pores of local particles. Accordingly, pore water pressure transducers are associated with the local soil response. However, the acceleration responses represent the whole-system responses, which are related to the dynamic responses at the macro scale. This fact corroborates the reason the measured r_u responses were slightly delayed compared to the estimated r_u responses from accelerometers.

Discussion and Limitations

Strain-based and energy-based methods are under the assumption of one-dimensional shear beam behavior of the soil, which corresponds to laboratory tests. Accordingly, laboratory tests, such as cyclic triaxial and direct simple shear tests, have demonstrated a strong relation between r_u and γ or $\Sigma\Delta W/\sigma'_{v0}$. These laboratory tests enable precise control of various factors, including soil

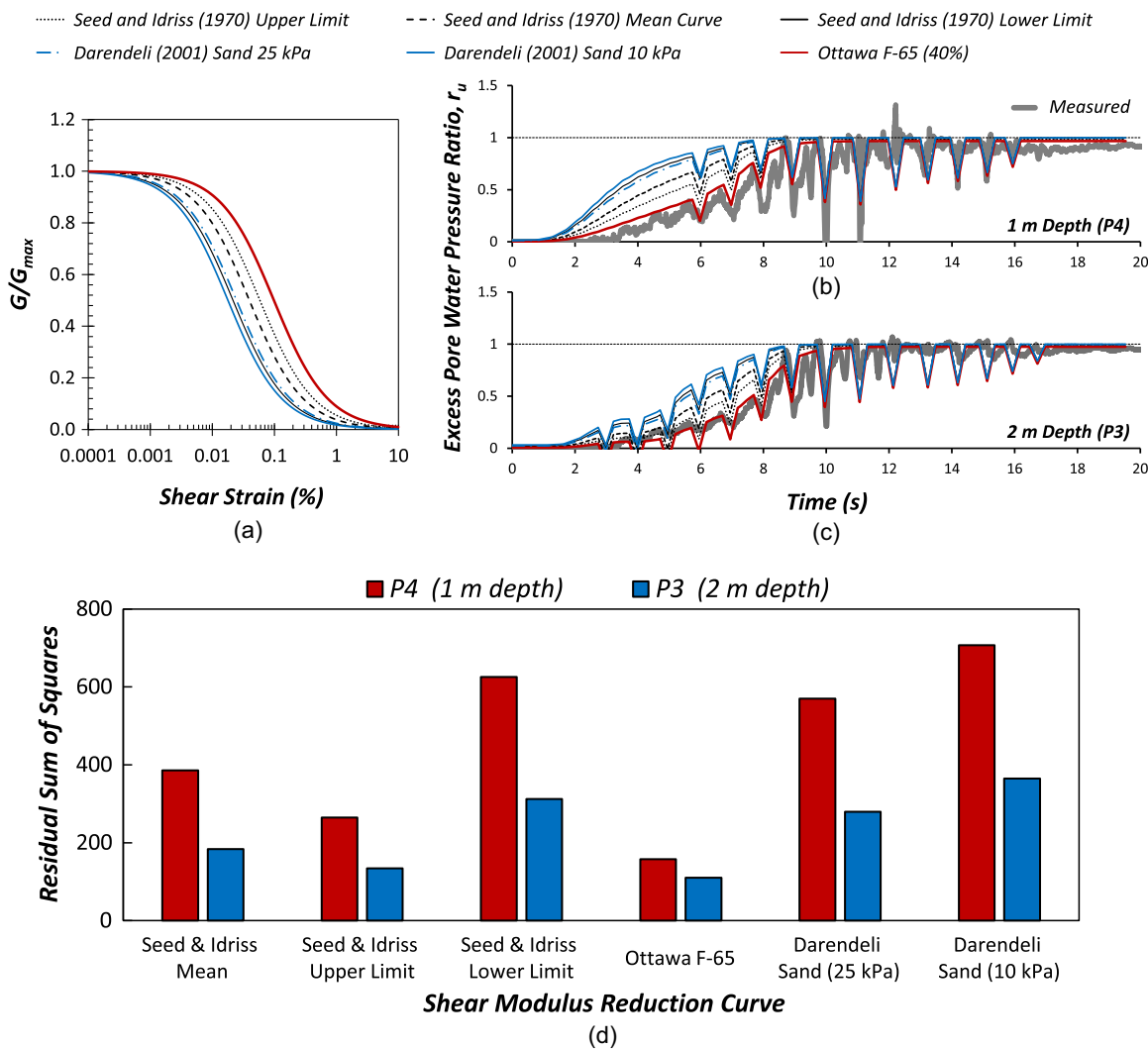


Fig. 14. Sensitivity analysis of shear modulus reduction curves for strain-based estimation: (a) shear modulus reduction curves for sensitivity analysis [Seed and Idriss 1970; Darendeli 2001; and Ottawa F-65 from Ramirez et al. (2018)]; (b) comparison of excess pore water pressure ratio between the measured and estimated responses from UCD2 at a depth of 1 m (P3); and (c) a depth of 2 m (P4); and (d) residual sum of squares between measured and estimated responses from UCD2 at a depth of 1 and 2 m.

properties, sensors, input excitation, and so on. This controlled environment enables laboratory tests suitable for representing small-scale soil behavior. On the other hand, field conditions are characterized by numerous uncertainties surpassing those encountered in laboratory tests. These uncertainties encompass factors such as soil layers, in situ soil conditions, soil anisotropy, soil heterogeneity, earthquake waves, and others. Moreover, the shear modulus reduction curves in the strain-based method and the presence of multi-layered soil deposits highlight uncertainties that can affect r_u estimation. This section delves into the sensitivity analysis of shear modulus reduction curves and height of the soil layer, both of which influence the estimation of r_u .

Sensitivity Analysis of Shear Modulus Reduction Curves for Strain-Based Method

The strain-based method requires a G/G_{\max} curve to estimate r_u . The timing varying strain $\gamma(t)$, as defined in Eq. (1), directly influences the computation of $r_u(t)$ according to Eq. (3). As a result, the selection of the G/G_{\max} curve significantly impacts the sensitivity of the strain-based method. To perform a sensitivity analysis

on G/G_{\max} curves for strain-based estimation, this study employed six representative curves for sand [Fig. 14(a)]: mean curve, upper and lower limit from Seed and Idriss (1970), two curves from Darendeli (2001), and Ottawa F-65, for a relative density of 40% which was previously used. Darendeli (2001) curves for sand were obtained using the following equations:

$$G/G_{\max} = \frac{1}{1 + \left(\frac{\gamma}{\gamma_R}\right)^{0.92}} \quad (11)$$

$$\gamma_R = (0.0352 + 0.0001 \cdot PI \cdot OCR^{0.33}) \left(\frac{\sigma'_{v0}}{P_a}\right)^{0.35} \quad (12)$$

where γ_R = reference strain in %; PI = plasticity index of soil; and OCR = overconsolidation ratio. Because the liquefaction primarily occurs in sandy soil, the shear modulus reduction curves from Darendeli (2001) were obtained by setting PI = 0 and OCR = 1 in Eq. (12). The curves were generated corresponding to σ'_{v0} of 10 and 25 kPa, which are similar to σ'_{v0} at 1 and 2 m depth in the centrifuge tests of LEAP.

The measured r_u responses at the depth of 1 and 2 m from UCD2 were used as benchmarks for the sensitivity analysis [Figs. 14(b and c)]. The estimated responses using the Ottawa sand curve closely aligned with the measured responses. The G/G_{\max} curves from Seed and Idriss (1970) and Darendeli (2001) exhibited a significant reduction in shear modulus within the strain range of 0.0001% to 0.01%. This amplified the r_u buildup at the onset of shaking between 2 and 6 s, particularly when dealing with changes in lower strain levels. The residual sum of squares (RSS) quantifies the difference between measured ($r_{u_measured}$) and estimated responses ($r_{u_estimated}$) according to the shear modulus curves [Fig. 14(d)]

$$RSS = \sum (r_{u_measured} - r_{u_estimated})^2 \quad (13)$$

The RSS analysis demonstrates that using the Ottawa F-65 curve results in a more accurate estimation of r_u . This difference becomes particularly significant when the chosen G/G_{\max} curve deviates substantially from the Ottawa F-65 sand curve. The ratio of G/G_{\max} significantly decreased as the soil became more well graded (Wichtmann and Triantafyllidis 2013). The Ottawa F-65 used for the centrifuge tests was a clean poorly graded sand made by US silica (ElGhoraiby et al. 2020), implying a higher G/G_{\max} value at certain shear strain levels compared to the other curves. Consequently, G/G_{\max} values from the literature, representing shear modulus reduction curves for typical sands, are not applicable for estimating r_u through the strain-based method in the context of centrifuge tests. The strain-based method necessitates the selection of an appropriate G/G_{\max} curve that corresponds to the specific target soil properties.

Sensitivity Analysis of the Height of Soil Layer

Strain-based and energy-based estimation significantly depend on how both methods define the soil layer based on acceleration records. For the centrifuge tests used for LEAP, if both methods do not use adjacent pairs of two accelerometers (e.g., AH4–AH3, AH3–AH2, AH2–AH1) for strain and energy calculation, estimated r_u responses could differ. Selection of a pair of accelerometers from centrifuge tests determines the specific soil layer of interest and consequently affects the height of the soil layer (h) and σ'_{v0} representing the target soil layer used to calculate γ , τ , and $\Sigma\Delta W/\sigma'_{v0}$ through Eqs. (1) and (5). In this context, a sensitivity analysis was conducted

for h , considering three cases from Ehime 3: (1) Case 1 using AH4 and AH1 with a vertical distance of 3 m; (2) Case 2 using AH4 and AH2 with a vertical distance of 2 m; and (3) Case 3 using AH4 and AH3 with a vertical distance of 1 m (Fig. 15).

The specific soil layers of interest exhibited different stress–strain responses according to the three cases from Ehime 3 [Figs. 15(a–c)]. As the difference between acceleration responses became pronounced with increasing h due to the site amplification, the shear stress increased with increasing h , indicating the thickening of the target soil layer. Conversely, in Case 3, the thinnest soil layer, a higher accumulation of shear strain occurred due to the smaller h , leading to a greater average shear strain calculation from Eq. (1). The $\Sigma\Delta W/\sigma'_{v0}$ over time is depicted in Fig. 15(d). The value of σ'_{v0} at the midpoint depth of the two accelerometers used for each case was used to normalize ΔW . The value of $\Sigma\Delta W/\sigma'_{v0}$ of Case 1 was notably less than that of the other two cases, whereas Cases 2 and 3 exhibited similar $\Sigma\Delta W/\sigma'_{v0}$.

The strain-based and energy-based methods estimate r_u for each case [Figs. 16(a and b)]. The r_u estimations from three cases were compared against the measured r_u responses at different depths (P2–P4) from Ehime 3. The RSS between $r_{u_measured}$ and $r_{u_estimated}$ was computed using Eq. (13) according to each case. This comparison was carried out separately for the strain-based [Fig. 16(c)] and energy-based methods [Fig. 16(d)]. The energy-based method exhibited significantly lower RSS values across all cases, indicating that it provided more accurate r_u estimations compared to the strain-based method. As shown in Fig. 15, the energy-based method captured stress and strain variations depending on the specific soil layer of interest, whereas the strain-based method only reflected changes in strain for the estimation. In order to effectively describe the shear beam response of the soil layer during soil liquefaction, the response of the soil layer should encompass both shear stress and strain simultaneously, a requirement that the strain-based method fell short of meeting. Meanwhile, in the energy-based method, Case 3 indicated the dynamic responses of the soil layer sandwiched between AH4 and AH3, so that Case 3 showed less RRS with P4, which was situated between AH4 and AH3. In contrast, Cases 1 and 2 exhibited less RRS with P3, situated near the midpoint of accelerometer pairs for Cases 1 and 2. This observation implies that the energy-based method better represents soil responses at the midpoint of the target layer.

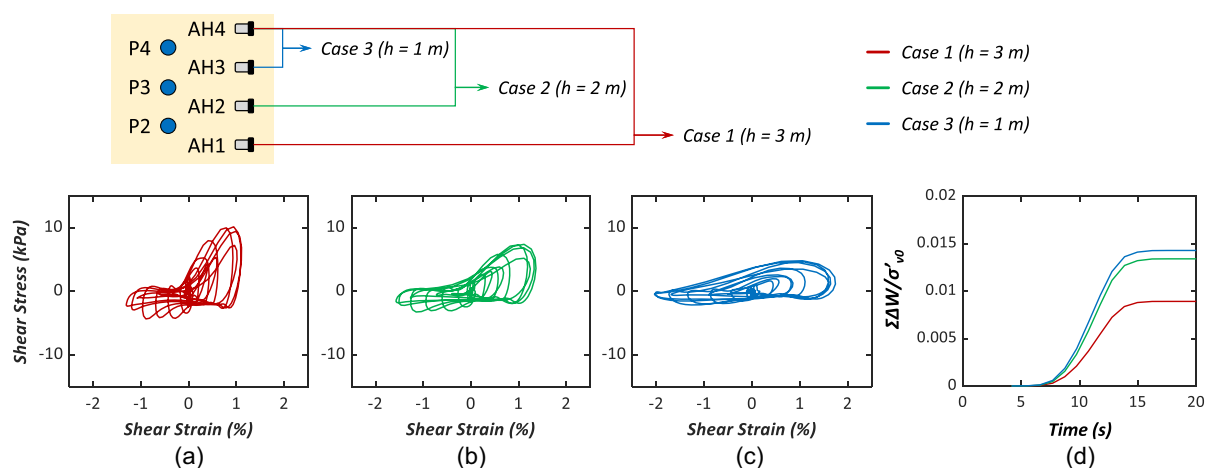


Fig. 15. Sensitivity analysis of the height of the soil layer using the centrifuge data from Ehime 3: shear strain and stress responses of (a) Case 1 using AH4 and AH1 ($h = 3$ m); (b) Case 2 using AH4 and AH2 ($h = 2$ m); (c) Case 3 using AH4 and AH1 ($h = 1$ m); and (d) normalized cumulative energy over time depending on cases.

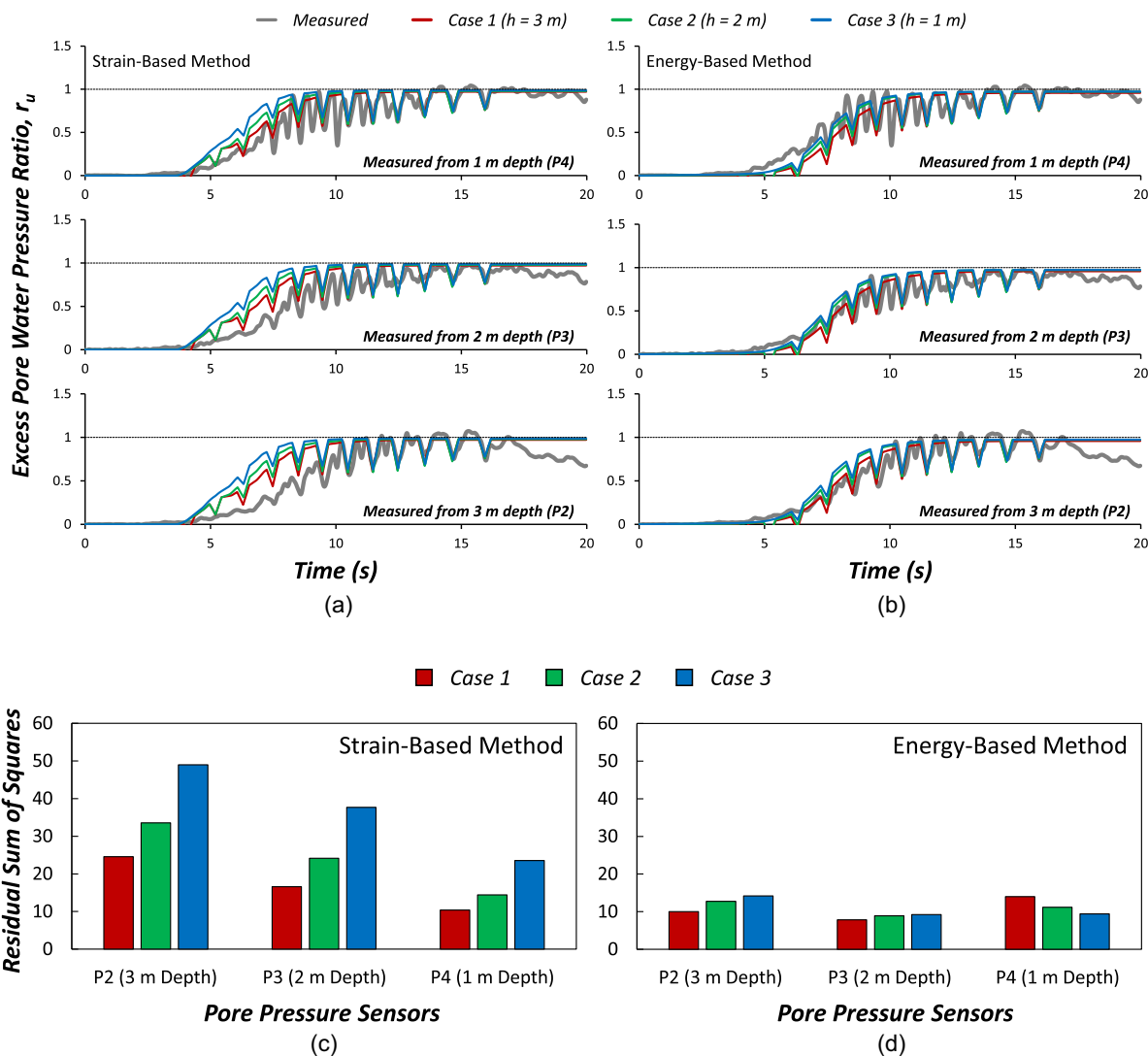


Fig. 16. Comparison of excess pore water pressure ratio between the measured and estimated responses from sensitivity analysis of the height of soil layer using the centrifuge data from Ehime 3: (a) strain-based estimation; (b) energy-based estimation; (c) residual sum of squares between measured and estimated responses through strain-based estimation; and (d) energy-based estimation.

Limitations of the Strain-Based and Energy-Based Methods

Both methods have their own advantages and limitations. The strain-based method requires only a little information relevant to the liquefiable soil layer, such as two acceleration records and a G/G_{\max} curve representing the soil behavior, whereas the energy-based method needs more information, such as two acceleration records, σ'_{v0} and ρ of the soil layer, and $\Sigma\Delta W/\sigma'_{v0}$ and r_u correlation. The strain-based method assumes nonlinear behavior of the soil following initial G/G_{\max} curves during the pore water pressure buildup, which inherently implies limitations. Because the energy-based method requires more information on the soil, the energy-based method provides a more accurate estimation of r_u than the strain-based method.

Both methods were developed based on the assumption of the one-dimensional shear beam behavior of soil without considering the effect of lateral stress variations in soil during earthquakes. Shear stress–strain responses from vertically aligned accelerometers represent averaged stress–strain responses of soil layers sandwiched between used accelerometers. Accordingly, the further

apart the used accelerometers are, and the more diverse the types of soil layers between the used accelerometers, the more the stress–strain responses computed by the two developed methods cannot represent the shear beam behavior of the entire soil layer, and ultimately, the estimated r_u becomes inaccurate.

As this study showed, these methods are more applicable for the centrifuge tests that had only a uniform soil layer. Although the empirical relations for the energy-based method were developed based on mildly sloping ground, which inherently incorporates the influence of an initial static shear stress on the cyclic strength, the estimated r_u was comparable to the responses measured in level ground results presented by Hayden et al. (2015). However, both methods should be carefully used when applying to the field cases involving uncertainties of multilayered soils, sloping ground, irregular earthquake waves, and so on. Moreover, these methods enable back-estimation of pore water pressure within liquefied soil only for the past event. These methods should be improved to predict pore water pressure for future events because the methods require specific acceleration time histories, which should represent the one-dimensional shear beam behavior of soil.

Conclusions

Undrained cyclic loading reduces the effective stress of the soil with excess pore water pressure generation, accumulates shear strain, and changes the shear modulus of the soil simultaneously. Accordingly, the changes in the liquefiable soil mechanical properties, such as the effective stress due to pore pressure generation, shear strain, and shear modulus, are compounded and interdependent on each other. This study developed and validated the methods of estimating the excess pore water pressure ratio using acceleration responses of the liquefiable soil: strain-based and energy-based estimation. The centrifuge test results from LEAP-UCD-2017 were used to create the empirical models for the estimation methods. The relative density of the soil differed from the employed centrifuge tests but under the same shaking intensity. For validation of the methods, the developed empirical models were applied to centrifuge tests, which had the same relative density under different shaking intensities as the centrifuge tests employed for the development. Moreover, the acceleration and pore water pressure responses from the case history, the 1987 Superstition Hills earthquake at the Wildlife site, facilitated validation of the methods. The main findings of this study are summarized as follows:

1. The generated excess pore water pressure ratio was proportional to the accumulated works by the shear stress–strain responses. The cumulative works were normalized by the vertical effective stress of the soil. The higher the relative density of the soil, the more energy was required to be liquefied, and this was consistent with the results from the laboratory tests in the previous literature.
2. The dilation behavior of the undrained soil during liquefaction generated a transient drop in the excess pore water pressure ratio and dilation spikes in the shear stress responses. A linear empirical equation in the logarithmic scale was developed for the relation between the excess pore water pressure ratio and induced peak shear stress normalized by the vertical effective stress of the soil. The lower the relative density of the soil, the more significant the transient drop in excess pore water pressure due to dilative behavior became.
3. The validation using centrifuge tests indicated that both methods well estimated the excess pore water pressure ratio. In general, the energy-based estimation successfully captured the measured pore pressure responses.
4. Both methods were applied to the case history, the 1987 Superstition Hills earthquake at the Wildlife site. In the N–S and E–W directions, both methods revealed the timing of the liquefaction much earlier than the measured excess pore water pressure ratio. However, the timing of the liquefaction from the estimation was comparable with that from the Stockwell transform. The excess pore water pressure might be slowly generated due to the migration of the pore pressure through the soil media, although the liquefaction occurred much earlier than the pore pressure ratio indicated.
5. The strain-based and energy-based methods require G/G_{\max} curves and the empirical equations associated with the dilative behavior and the relation between the cumulative dissipated energy and excess pore water pressure ratio. The necessary curves and equations significantly affect the estimation results, so the empirical equations for each soil should be developed through laboratory tests or numerical studies in the future.
6. This study is primarily applicable to uniform soil layers, where it becomes possible to simplify liquefiable soil as the one-dimensional shear beam. Consequently, the proposed methods find greater relevance in centrifuge tests, which commonly consist of poorly graded sand and provide more precise information

about the soil layer, including the height of the layer of interest and G/G_{\max} curves.

Data Availability Statement

Some or all data, models, or code that support the findings of this study are available from the corresponding author upon reasonable request.

Acknowledgments

The Department of Civil and Environmental Engineering at the University of California, Berkeley, is thanked for supporting Dr. Ko as a postdoctoral visiting scholar. The authors appreciate Prof. Kokusho, who provided valuable insight associated with energy-based soil liquefaction evaluation.

References

- Bartlett, S. F., and T. L. Youd. 1995. "Empirical prediction of liquefaction-induced lateral spread." *J. Geotech. Eng.* 121 (4): 316–329. [https://doi.org/10.1061/\(ASCE\)0733-9410\(1995\)121:4\(316\)](https://doi.org/10.1061/(ASCE)0733-9410(1995)121:4(316)).
- Berrill, J. B., and R. O. Davis. 1985. "Energy dissipation and seismic liquefaction of sands: Revised model." *Soils Found.* 25 (2): 106–118. https://doi.org/10.3208/sandf1972.25.2_106.
- Boulanger, R. W., and I. M. Idriss. 2012. "Probabilistic standard penetration test–based liquefaction–triggering procedure." *J. Geotech. Geoenviron. Eng.* 138 (10): 1185–1195. [https://doi.org/10.1061/\(ASCE\)GT.1943-5606.0000700](https://doi.org/10.1061/(ASCE)GT.1943-5606.0000700).
- Cetin, K. O., R. B. Seed, A. der Kiureghian, K. Tokimatsu, L. F. Harder, R. E. Kayen, and R. E. S. Moss. 2004. "Standard penetration test–based probabilistic and deterministic assessment of seismic soil liquefaction potential." *J. Geotech. Geoenviron. Eng.* 130 (12): 1314–1340. [https://doi.org/10.1061/\(ASCE\)1090-0241\(2004\)130:12\(1314\)](https://doi.org/10.1061/(ASCE)1090-0241(2004)130:12(1314)).
- Cetin, K. O., R. B. Seed, R. E. Kayen, R. E. S. Moss, H. T. Bilge, M. Ilgac, and K. Chowdhury. 2018. "SPT-based probabilistic and deterministic assessment of seismic soil liquefaction triggering hazard." *Soil Dyn. Earthquake Eng.* 115 (Apr): 698–709. <https://doi.org/10.1016/j.soildyn.2018.09.012>.
- Chandra, J., P. Guéguen, J. H. Steidl, and L. F. Bonilla. 2015. "In situ assessment of the $G-\gamma$ curve for characterizing the nonlinear response of soil: Application to the Garner Valley downhole array and the Wildlife liquefaction array." *Bull. Seismol. Soc. Am.* 105 (2A): 993–1010. <https://doi.org/10.1785/0120140209>.
- Darendeli, M. B. 2001. "Development of a new family of normalized modulus reduction and material damping curves." Ph.D. dissertation, Dept. of Civil, Architectural, and Environmental Engineering, Univ. of Texas at Austin.
- Dobry, R., R. Ladd, F. Yokel, R. Chung, and D. Powell. 1982. *Prediction of pore water pressure buildup and liquefaction of sands during earthquakes by the cyclic strain method*. NBS Building Science Series 138. Washington, DC: National Bureau of Standards.
- Egan, J. A., and D. Rosidi. 1991. "Assessment of earthquake-induced liquefaction using ground-motion energy characteristics." In *Proc., Pacific Conf. on Earthquake Engineering*, Christchurch, New Zealand: New Zealand National Society for Earthquake Engineering.
- ElGhoraiby, M. A., H. Park, and M. T. Manzari. 2020. "Stress–strain behavior and liquefaction strength characteristics of Ottawa F65 sand." *Soil Dyn. Earthquake Eng.* 138 (Apr): 106292. <https://doi.org/10.1016/j.soildyn.2020.106292>.
- El-Sekelly, W., R. Dobry, T. Abdoun, and J. H. Steidl. 2017. "Two case histories demonstrating the effect of past earthquakes on liquefaction resistance of silty sand." *J. Geotech. Geoenviron. Eng.* 143 (6): 04017009. [https://doi.org/10.1061/\(ASCE\)GT.1943-5606.0001654](https://doi.org/10.1061/(ASCE)GT.1943-5606.0001654).
- Figuroa, J. L., A. S. Saada, L. Liang, and N. M. Dahisaria. 1994. "Evaluation of soil liquefaction by energy principles." *J. Geotech. Eng.*

- 120 (9): 1554–1569. [https://doi.org/10.1061/\(ASCE\)0733-9410\(1994\)120:9\(1554\)](https://doi.org/10.1061/(ASCE)0733-9410(1994)120:9(1554)).
- Garnier, J., C. Gaudin, S. M. Springman, P. J. Culligan, D. Goodings, D. König, B. Kutter, R. Phillips, M. F. Randolph, and L. Thorel. 2007. “Catalogue of scaling laws and similitude questions in geotechnical centrifuge modeling.” *Int. J. Phys. Modell. Geotech.* 7 (3): 1–23. <https://doi.org/10.1680/ijpmg.2007.070301>.
- Green, R. A., J. K. Mitchell, and C. P. Polito. 2000. “An energy-based pore pressure generation model for cohesionless soils.” In *Proc., John Booker Memorial Symp.—Developments in Theoretical Geomechanics*, edited by D. W. Smith and J. P. Carter, 383–390. Rotterdam, Netherlands: A. A. Balkema.
- Haag, E. D., and K. H. Stokoe II. 1985. *Laboratory investigation of static and dynamic properties of sandy soils subjected to the 1981 Westmorland earthquake*. Research Rep. No. GR85-11. Austin, TX: Univ. of Texas.
- Haddadi, H., A. Shakal, C. Stephens, W. Savage, M. Huang, W. Leith, and J. Parrish. 2008. “Center for engineering strong-motion data (CESMD).” In *Proc., 14th World Conf. on Earthquake Engineering*. Tokyo: International Association for Earthquake Engineering.
- Hayden, C., J. Allmond, I. Rawlings, B. Kutter, J. Bray, T. Hutchinson, G. Fiegel, J. Zupan, and A. Whittaker. 2013. *Test-6: Six elastic model structures on a layered, saturated soil profile*. Austin, TX: DesignSafe-CI. <https://doi.org/10.4231/D3QF8J99>.
- Hayden, C. P., J. D. Zupan, J. D. Bray, J. D. Allmond, and B. L. Kutter. 2015. “Centrifuge tests of adjacent mat-supported buildings affected by liquefaction.” *J. Geotech. Geoenviron. Eng.* 141 (3): 04014118. [https://doi.org/10.1061/\(ASCE\)GT.1943-5606.0001253](https://doi.org/10.1061/(ASCE)GT.1943-5606.0001253).
- Hutabarat, D., and J. D. Bray. 2019. “Effective stress analysis of liquefiable site in Christchurch to discern the characteristics of sediment ejecta.” In *Proc., Earthquake Geotechnical Engineering for Protection and Development of Environment and Constructions*, edited by F. Silvestri and N. Moraci, 2923–2931. Rome: Italian Geotechnical Association.
- Idriss, I. M., and R. W. Boulanger. 2008. *Soil liquefaction during earthquakes*. Oakland, CA: Earthquake Engineering Research Institute.
- Ishihara, K. 1993. “Liquefaction and flow failure during earthquakes.” *Géotechnique* 43 (3): 351–451. <https://doi.org/10.1680/geot.1993.43.3.351>.
- Ishihara, K., and Y. Koga. 1981. “Case studies of liquefaction in the 1964 Niigata earthquake.” *Soils Found.* 21 (3): 35–52. https://doi.org/10.3208/sandf1972.21.3_35.
- Kayen, R., R. E. S. Moss, E. M. Thompson, R. B. Seed, K. O. Cetin, A. der Kiureghian, Y. Tanaka, and K. Tokimatsu. 2013. “Shear-wave velocity-based probabilistic and deterministic assessment of seismic soil liquefaction potential.” *J. Geotech. Geoenviron. Eng.* 139 (3): 407–419. [https://doi.org/10.1061/\(ASCE\)GT.1943-5606.0000743](https://doi.org/10.1061/(ASCE)GT.1943-5606.0000743).
- Kayen, R. E., and J. K. Mitchell. 1997. “Assessment of liquefaction potential during earthquakes by Arias intensity.” *J. Geotech. Geoenviron. Eng.* 123 (12): 1162–1174. [https://doi.org/10.1061/\(ASCE\)1090-0241\(1997\)123:12\(1162\)](https://doi.org/10.1061/(ASCE)1090-0241(1997)123:12(1162)).
- Kokusho, T. 2013. “Liquefaction potential evaluations: Energy-based method versus stress-based method.” *Can. Geotech. J.* 50 (10): 1088–1099. <https://doi.org/10.1139/cgj-2012-0456>.
- Kokusho, T. 2014. “Seismic base-isolation mechanism in liquefied sand in terms of energy.” *Soil Dyn. Earthquake Eng.* 63 (Apr): 92–97. <https://doi.org/10.1016/j.soildyn.2014.03.015>.
- Kokusho, T. 2021. “Energy-based liquefaction evaluation for induced strain and surface settlement—Evaluation steps and case studies” *Soil Dyn. Earthquake Eng.* 143 (Sep): 106552. <https://doi.org/10.1016/j.soildyn.2020.106552>.
- Kokusho, T., and S. Tanimoto. 2021. “Energy capacity versus liquefaction strength investigated by cyclic triaxial tests on intact soils.” *J. Geotech. Geoenviron. Eng.* 147 (4): 04021006. [https://doi.org/10.1061/\(ASCE\)GT.1943-5606.0002484](https://doi.org/10.1061/(ASCE)GT.1943-5606.0002484).
- Kostadinov, M. V., and F. Yamazaki. 2001. “Detection of soil liquefaction from strong motion records.” *Earthquake Eng. Struct. Dyn.* 30 (2): 173–193. [https://doi.org/10.1002/1096-9845\(200102\)30:2<173::AID-EQE3>3.0.CO;2-7](https://doi.org/10.1002/1096-9845(200102)30:2<173::AID-EQE3>3.0.CO;2-7).
- Kramer, S. L., S. S. Sideras, and M. W. Greenfield. 2016. “The timing of liquefaction and its utility in liquefaction hazard evaluation.” *Soil Dyn. Earthquake Eng.* 91 (Sep): 133–146. <https://doi.org/10.1016/j.soildyn.2016.07.025>.
- Kutter, B. L., M. T. Manzari, and M. Zeghal. 2020. *Model tests and numerical simulations of liquefaction and lateral spreading: LEAP-UCD-2017*. New York: Springer.
- Kutter, B. L., and D. W. Wilson. 1999. “De-liquefaction shock waves.” In *Proc., 7th US–Japan Workshop on Earthquake Resistant Design of Lifeline Facilities and Countermeasures against Soil Liquefaction*, edited by T. D. O’Rourke, J. P. Bardet, and M. Hamada, 295–310. Buffalo, NY: State Univ. of New York.
- Manandhar, S., S. Kim, J. Ha, K. Ko, M. Lee, and S. Kim. 2021. “Liquefaction evaluation using frequency characteristics of acceleration records in KAIST centrifuge tests for LEAP.” *Soil Dyn. Earthquake Eng.* 140 (Jun): 106332. <https://doi.org/10.1016/j.soildyn.2020.106332>.
- Millen, M. D. L., A. Viana da Fonseca, and C. M. Azeredo. 2021. “Time-frequency filter for computation of surface acceleration for liquefiable sites: Equivalent linear Stockwell analysis method.” *J. Geotech. Geoenviron. Eng.* 147 (8): 04021070. [https://doi.org/10.1061/\(ASCE\)GT.1943-5606.0002581](https://doi.org/10.1061/(ASCE)GT.1943-5606.0002581).
- Moss, R. E., R. B. Seed, R. E. Kayen, J. P. Stewart, A. der Kiureghian, and K. O. Cetin. 2006. “CPT-based probabilistic and deterministic assessment of in situ seismic soil liquefaction potential.” *J. Geotech. Geoenviron. Eng.* 132 (8): 1032–1051. [https://doi.org/10.1061/\(ASCE\)1090-0241\(2006\)132:8\(1032\)](https://doi.org/10.1061/(ASCE)1090-0241(2006)132:8(1032)).
- NAS (National Academies of Sciences, Engineering, and Medicine). 2021. *State of the art and practice in the assessment of earthquake-induced soil liquefaction and its consequences*. Washington, DC: National Academies Press. <https://doi.org/10.17226/23474>.
- Nemat-Nasser, S., and A. Shokooh. 1979. “A unified approach to densification and liquefaction of cohesionless sand in cyclic shearing.” *Can. Geotech. J.* 16 (4): 659–678. <https://doi.org/10.1139/t9-076>.
- NIED (National Research Institute for Earth Science and Disaster Resilience). 2019. *NIED K-NET, KiK-net*. Tsukuba, Japan: NIED. <https://doi.org/10.17598/NIED.0004>.
- Polito, C. P., R. A. Green, and J. Lee. 2008. “Pore pressure generation models for sands and silty soils subjected to cyclic loading.” *J. Geotech. Geoenviron. Eng.* 134 (10): 1490–1500. [https://doi.org/10.1061/\(ASCE\)1090-0241\(2008\)134:10\(1490\)](https://doi.org/10.1061/(ASCE)1090-0241(2008)134:10(1490)).
- Polito, C. P., and J. R. Martin II. 2001. “Effects of nonplastic fines on the liquefaction resistance of sands.” *J. Geotech. Geoenviron. Eng.* 127 (5): 408–415. [https://doi.org/10.1061/\(ASCE\)1090-0241\(2001\)127:5\(408\)](https://doi.org/10.1061/(ASCE)1090-0241(2001)127:5(408)).
- Ramirez, J., A. R. Barrero, L. Chen, S. Dashti, A. Ghofrani, M. Taiebat, and P. Arduino. 2018. “Site response in a layered liquefiable deposit: Evaluation of different numerical tools and methodologies with centrifuge experimental results.” *J. Geotech. Geoenviron. Eng.* 144 (10): 04018073. [https://doi.org/10.1061/\(ASCE\)GT.1943-5606.0001947](https://doi.org/10.1061/(ASCE)GT.1943-5606.0001947).
- Roesler, S. K. 1979. “Anisotropic shear modulus due to stress anisotropy.” *J. Geotech. Eng. Div.* 105 (7): 871–880. <https://doi.org/10.1061/AJGEB6.0000835>.
- Schofield, A. N. 1980. “Cambridge geotechnical centrifuge operations.” *Géotechnique* 30 (3): 227–268. <https://doi.org/10.1680/geot.1980.30.3.227>.
- Seed, H. B., and I. M. Idriss. 1970. *Soil moduli and damping factors for dynamic response analyses*. Berkeley, CA: Univ. of California.
- Seed, H. B., and I. M. Idriss. 1971. “Simplified procedure for evaluating soil liquefaction potential.” *J. Soil Mech. Found. Div.* 97 (9): 1249–1273. <https://doi.org/10.1061/JSEFAQ.0001662>.
- Seed, H. B., K. Tokimatsu, L. F. Harder, and R. M. Chung. 1985. “Influence of SPT procedures in soil liquefaction resistance evaluations.” *J. Geotech. Eng.* 111 (12): 1425–1445. [https://doi.org/10.1061/\(ASCE\)0733-9410\(1985\)111:12\(1425\)](https://doi.org/10.1061/(ASCE)0733-9410(1985)111:12(1425)).
- Selig, E., K. Simcock, R. Davis, J. Berrill, and G. Mullenger. 1983. “Cyclic triaxial tests with continuous measurement of dissipated energy.” *Geotech. Test. J.* 6 (1): 35. <https://doi.org/10.1520/GTJ10822J>.
- Steidl, J., and P. Hegarty. 2017. “Instrumented field sites and liquefaction monitoring in the United States.” In *Proc., 16th World Conf. on Earthquake Engineering*. Tokyo: International Association for Earthquake Engineering.

- Towhata, I., and K. Ishihara. 1985. "Shear work and pore water pressure in undrained shear." *Soils Found.* 25 (3): 73–84. https://doi.org/10.3208/sandf1972.25.3_73.
- Unjoh, S., M. Kaneko, S. Kataoka, K. Nagaya, and K. Matsuoka. 2012. "Effect of earthquake ground motions on soil liquefaction." *Soils Found.* 52 (5): 830–841. <https://doi.org/10.1016/j.sandf.2012.11.006>.
- Wichtmann, T., and T. Triantafyllidis. 2013. "Effect of uniformity coefficient on G/G_{\max} and damping ratio of uniform to well-graded quartz sands." *J. Geotech. Geoenviron. Eng.* 139 (1): 59–72. [https://doi.org/10.1061/\(ASCE\)GT.1943-5606.0000735](https://doi.org/10.1061/(ASCE)GT.1943-5606.0000735).
- Youd, T. L., et al. 2001. "Liquefaction resistance of soils: Summary report from the 1996 NCEER and 1998 NCEER/NSF workshops on evaluation of liquefaction resistance of soils." *J. Geotech. Geoenviron. Eng.* 127 (10): 817–833. [https://doi.org/10.1061/\(ASCE\)1090-0241\(2001\)127:10\(817\)](https://doi.org/10.1061/(ASCE)1090-0241(2001)127:10(817)).
- Youd, T. L., and B. L. Carter. 2005. "Influence of soil softening and liquefaction on spectral acceleration." *J. Geotech. Geoenviron. Eng.* 131 (7): 811–825. [https://doi.org/10.1061/\(ASCE\)1090-0241\(2005\)131:7\(811\)](https://doi.org/10.1061/(ASCE)1090-0241(2005)131:7(811)).
- Zeghal, M., et al. 2018. "Stress–strain response of the LEAP-2015 centrifuge tests and numerical predictions." *Soil Dyn. Earthquake Eng.* 113 (Feb): 804–818. <https://doi.org/10.1016/j.soildyn.2017.10.014>.
- Zeghal, M., and A. Elgamal. 1994. "Analysis of site liquefaction using earthquake records." *J. Geotech. Eng.* 120 (6): 996–1017. [https://doi.org/10.1061/\(ASCE\)0733-9410\(1994\)120:6\(996\)](https://doi.org/10.1061/(ASCE)0733-9410(1994)120:6(996)).